



Search for new physics in top quark production with additional leptons in proton-proton collisions at $\sqrt{s} = 13$ TeV using effective field theory

The CMS Collaboration*

Abstract

Events containing one or more top quarks produced with additional prompt leptons are used to search for new physics within the framework of an effective field theory (EFT). The data correspond to an integrated luminosity of 41.5 fb^{-1} of proton-proton collisions at a center-of-mass energy of 13 TeV at the LHC, collected by the CMS experiment in 2017. The selected events are required to have either two leptons with the same charge or more than two leptons; jets, including identified bottom quark jets, are also required, and the selected events are divided into categories based on the multiplicities of these objects. Sixteen dimension-six operators that can affect processes involving top quarks produced with additional charged leptons are considered in this analysis. Constructed to target EFT effects directly, the analysis applies a novel approach in which the observed yields are parameterized in terms of the Wilson coefficients (WCs) of the EFT operators. A simultaneous fit of the 16 WCs to the data is performed and two standard deviation confidence intervals for the WCs are extracted; the standard model expectations for the WC values are within these intervals for all of the WCs probed.

Submitted to the Journal of High Energy Physics

1 Introduction

There are numerous motivations to search for new particles or interactions at the CERN LHC. The strong evidence for dark matter [1, 2] and dark energy [3] suggests the possibility that the full list of nature’s constituents has not yet been discovered. Likewise, the observed asymmetry between matter and antimatter in the universe implies an additional source of CP violation [4]. Many explanations for the hierarchy between the Planck mass and the electroweak scale set by the vacuum expectation value of the Higgs field also include new particles [5–7]. Nonetheless, there is no guarantee that new particles exist in the mass range directly accessible at the LHC. To extend the discovery reach of the LHC, it is therefore important to consider not only direct searches for new particles, but also indirect means of probing higher energy scales.

One flexible framework for undertaking such indirect probes is that of effective field theory (EFT) [8–10]. An EFT is a low-energy approximation for a more fundamental theory involving interactions at a mass scale Λ . Treating the standard model (SM) as a low-energy approximation of a higher-energy theory, one can add additional higher-order terms to the Lagrangian consistent with the symmetries and conservation laws that expand the possibilities compatible with new physics at higher mass scales. The additional terms are constructed from operators—products of fields and their derivatives—that involve only SM fields. The EFT Lagrangian can then be written as

$$\mathcal{L}_{\text{EFT}} = \mathcal{L}_{\text{SM}} + \sum_{d,i} \frac{c_i^d}{\Lambda^{d-4}} \mathcal{O}_i^d, \quad (1)$$

where \mathcal{L}_{SM} is the SM Lagrangian, \mathcal{O}_i^d are the EFT operators of dimension d , and c_i^d are dimensionless parameters known as Wilson coefficients (WCs) that characterize the strength of the interactions at dimension d . The contribution of an operator of dimension d to the Lagrangian is suppressed by a factor of $1/\Lambda^{d-4}$ implying that the focus should be placed on operators of the lowest possible dimension. However, all operators of odd dimension violate baryon or lepton number [11], so dimension-five operators are neglected, and dimension-six operators provide the leading contribution from new physics [9]. The first sub-leading contributions that conserve baryon and lepton number arise from dimension-eight operators and are not considered in this analysis.

While the impact of EFT operators can in principle be detected in a large variety of experimental observables, it is particularly interesting to consider their impact on the production of one or more top quarks in association with additional leptons. In the SM, the leading contribution to this signature arises from the production of top quarks in association with a W , Z , or Higgs boson (H) [4]. It has long been speculated that the large mass of the top quark [12, 13], and hence its large coupling to the Higgs boson, might be an indication of a special relationship between the top quark and the physics of electroweak symmetry breaking. If so, the production of top quarks along with electroweak or Higgs bosons may shed some light on possible new dynamics. Only recently have experimental measurements started to test directly the coupling of the top quark to H [14, 15] and Z [16–18] bosons. The current and future LHC data therefore provide intriguing opportunities to study these processes in more detail. Furthermore, because of the new terms added within the EFT expansion, it is possible to consider the production of top quarks with additional leptons directly through four-fermion operators that do not contain H , W , or Z bosons. Such contributions are also probed as part of this analysis.

Collisions producing one or more top quarks and additional leptons generate a variety of signatures involving multiple leptons and jets, including jets that are initiated from the hadronization of bottom quarks, referred to as b jets. Top quarks decay with almost 100% branching fraction to a bottom quark and a W boson [4], which can decay either leptonically, to a charged

lepton and a neutrino, or hadronically, to two jets. If H, W, or Z bosons are produced in association with the top quarks, they may also decay in various ways involving quarks (including b quarks, especially in the case of the Higgs boson) or leptons. Ultimately, the final-state signatures are primarily determined by the decay modes of the bosons, either hadronic or leptonic. Final states in which multiple bosons decay leptonically present a number of experimental advantages. Multiple leptons provide an efficient trigger strategy, which remains viable even at large instantaneous luminosities. Furthermore, for final states involving either a same-charge dilepton pair or more than two leptons with additional jets (including b jets), the contributions from background processes are small compared to the size of the signals. These final states are the focus of this analysis and are denoted multilepton final states hereafter.

Focusing on multilepton final states leads to unique challenges that have not been encountered by previous LHC analyses employing EFT methods to search for new physics associated with top quark production [16, 18–27]. First, multilepton final states receive contributions from multiple processes, and it is not possible to isolate high-purity samples from each contribution. For example, both $t\bar{t}Z$ and electroweak tZq events contribute to the three-lepton final state where two of the leptons form a same-flavor, oppositely charged pair with an invariant mass near the Z boson mass peak. Likewise, same-charge dilepton and trilepton final states outside the Z peak originate with comparable probability from SM $t\bar{t}W$ and $t\bar{t}H$ production. Since the multiple processes cannot be reliably disentangled, this analysis cannot be constructed as a reinterpretation of either a set of inclusive or differential cross section measurements. Second, there are numerous EFT operators capable of impacting one or more of the processes contributing to multilepton final states; a priori, there is no reason to assume that new physics would manifest only through the contribution of a single operator. It is therefore important to analyze the effects of these operators simultaneously across all components of the data set.

A new approach is implemented to address these challenges. Designed to target EFT effects directly, this approach does not aim to isolate specific physical processes and extract high-level observables; rather, it relies on detector-level observables, namely the number of events observed in a set of distinct categories defined by the multiplicities of final-state objects. For each category, a different admixture of physics processes will contribute to the observed event yield. Sensitivity to the EFT operators is obtained by parameterizing the predicted yields in terms of the WCs of all relevant operators simultaneously. To procure these predicted yields, we use simulated events with weights parameterized to represent the effects of the EFT operators. These weighted, simulated events are then analyzed to obtain the necessary predictions of the observed event yields, as functions of the EFT parameters. Parameterizing the event weights in terms of the WCs represents the key enabling concept of this approach, as it allows all relevant interference effects—both interference between new physics and the SM and interference among new physics operators—to be incorporated into the prediction. The effects of multiple EFT operators on multiple physical processes contributing to a single final-state signature are therefore accounted for in a straightforward and rigorous manner. EFT operators can also impact the kinematical properties of the events, so this approach allows the full effect on the detector acceptance and efficiency to be appropriately described. Correlations among statistical and systematic uncertainties can also be accounted for, and, where possible, fully leveraged. For example, this approach should provide enhanced sensitivity when EFT operators impact the contribution of multiple relevant physics processes, since the observables used are sensitive to the sum of the effects. The main drawback of this approach is that, because it relies on detector-level observation and fully simulated events, theoretical updates cannot be incorporated without repeating the analysis. This is the first time such an approach has been applied to LHC data; ultimately, the technique can be applied to differential kinematical distributions,

but for this initial analysis, we take a more inclusive approach.

The detailed strategy employed in this analysis is as follows. Multilepton events are divided into categories based on the number and the sign of the charge sum of the reconstructed leptons; the lepton categories are then subdivided according to the number of b jets. Within each lepton and b jet category, the event yields are characterized as a function of the number of jets. For oppositely charged, same-flavor lepton pairs in three-lepton events, the data are divided based on whether the invariant mass of the lepton pair falls in a window around the Z boson mass (m_Z). This strategy results in 35 nonoverlapping categories. These event yields define the observables for the analysis and are compared against predictions that incorporate the effects of EFT operators. Contributions involving primarily prompt leptons—including signal processes—are modeled using simulated events. Where relevant, the predicted yields for processes sensitive to EFT operators are parameterized in terms of the WCs for those operators. Predictions for backgrounds involving primarily nonprompt leptons (e.g., leptons from bottom or charmed hadron decays or misidentified leptons) are based on extrapolations from control regions in data. The WCs are varied to determine the best fit of the predictions to data, as well as to establish the range over which the predicted yields are consistent with the observation.

The sections of the paper are organized in the following order. A brief overview of the CMS detector and triggering system is outlined in Section 2. Section 3 describes the simulation of signal and background processes, including a discussion of the parameterization of the predicted yields in terms of the WCs. The event reconstruction and event selection are covered in Sections 4 and 5, respectively, while Section 6 discusses the background estimation. In Section 7, the signal extraction is explained. Sources of systematic uncertainties affecting this analysis are described in Section 8. Section 9 presents the results, and Section 10 provides a summary of the analysis.

2 The CMS detector

The central feature of the CMS apparatus is a superconducting solenoid of 6 m internal diameter, providing a magnetic field of 3.8 T. Within the solenoid volume are a silicon pixel and strip tracker, a lead tungstate crystal electromagnetic calorimeter (ECAL), and a brass and scintillator hadron calorimeter (HCAL), each composed of a barrel and two endcap sections. Forward calorimeters extend the pseudorapidity coverage provided by the barrel and endcap detectors. Muons are detected in gas-ionization chambers embedded in the steel flux-return yoke outside the solenoid. A more detailed description of the CMS detector and its performance, together with a definition of the coordinate system and the kinematic variables used in the analysis, can be found in Ref. [28].

Events of interest are selected using a two-tiered trigger system [29]. The first level, composed of custom hardware processors, uses information from the calorimeters and muon detectors to select events at a rate of around 100 kHz within a fixed time interval of about 4 μ s. The second level, known as the high-level trigger, consists of a farm of processors running a version of the full event reconstruction software optimized for fast processing, and reduces the event rate to around 1 kHz before data storage.

3 Data samples and simulation

The data used in this analysis comprise proton-proton (pp) collisions at $\sqrt{s} = 13$ TeV collected with the CMS detector in 2017, corresponding to a total integrated luminosity of 41.5 fb⁻¹ [30].

The events have been recorded using a combination of single-, double-, and triple-lepton triggers.

Simulations are used to estimate the event yields of the signal processes and some sources of background. The signal samples incorporate EFT effects and are generated at leading order (LO), while all background samples are generated at next-to-leading order (NLO) and do not include EFT effects. The simulated samples used to estimate the backgrounds include $t\bar{t}\gamma$, diboson, and triboson production. Used for validation purposes, additional samples are also generated to simulate SM background processes that are estimated from data; these include Z+jets, W+jets, $t\bar{t}$ +jets, and single top quark processes (s channel, t channel, and tW). The background samples are generated using matrix elements (MEs) implemented either in the MADGRAPH5_aMC@NLO [31–33] (version 2.4.2) or the POWHEG v2 [34–40] programs. The simulation of the signal processes is described in Section 3.1

Parton showering and hadronization for all of the samples is done by PYTHIA [41] (version 8.226 was used for the signal samples), and the Lund fragmentation model is employed [42]. The parameters for the underlying event description correspond to the CP5 tune [43] and the proton structure is described by the NNPDF3.1 [44] set of parton distribution functions (PDFs). Minimum bias pp interactions occurring in the same or nearby bunch crossings (pileup) are generated with PYTHIA and overlaid on all simulated events, according to the luminosity profile of the analyzed data. Finally, all generated events are passed through a detailed simulation of the CMS apparatus, based on GEANT4 [45], and are reconstructed using the same event reconstruction software as used for data.

3.1 Simulation of the signal processes

The signal events are generated at LO with MADGRAPH5_aMC@NLO (version 2.6.0). The signal processes include those in which one or more top quarks are produced along with multiple charged leptons: $t\bar{t}l\bar{l}$, $t\bar{t}lq$, and $t\bar{t}l\nu$ (where l indicates a charged lepton and ν indicates a neutrino). We also include $t\bar{t}H$ and tHq , as these processes can produce signal events when the Higgs boson decays into one or more leptons. The decays of the Higgs bosons are handled by PYTHIA since it would be computationally expensive to produce MADGRAPH5_aMC@NLO samples for each decay mode and difficult to separate them from the other signal processes. An example diagram for each signal process is shown in Fig. 1. We note that the signal processes include contributions from lepton pairs produced from on-shell W and Z bosons, as well as those from nonresonant processes; this is important so that effects from EFT four-fermion operators can also be included in these samples. Furthermore, we note that the $t\bar{t}l\bar{l}$ sample includes the production of top quark pairs in association with virtual photons.

Sixteen operators are considered in this analysis. Chosen because they are expected to have a relatively large impact on the signal processes but not on the $t\bar{t}$ background process, the operators can be classified into two categories: operators that involve two quarks and one or more bosons, and operators that involve two quarks and two leptons. Table 1 lists the 16 operators and corresponding WCs; all couplings are assumed to involve only quarks of the third generation. The operators that require a Hermitian conjugate term in the Lagrangian (marked with a double dagger in Table 1) can have complex WCs; however, the imaginary coefficients lead to CP violation, and, as outlined in Ref. [46], are generally already constrained. Consequently, only the real components are considered in this analysis. More details about the operators listed in Table 1 can be found in Ref. [46]. For the purpose of illustrating which processes are most strongly affected by the operators considered, Table 1 lists the leading signal processes affected by each operator. To determine whether a process is to be listed in this

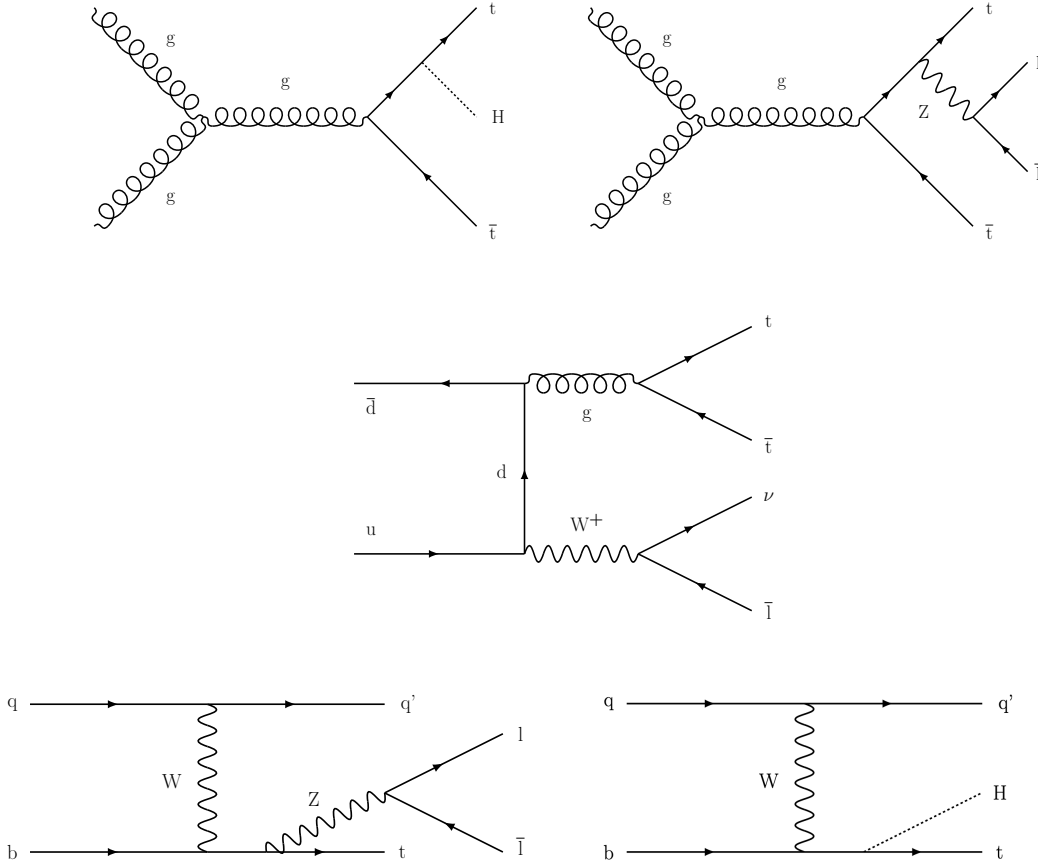


Figure 1: Example diagrams for the five signal processes considered in this analysis: $t\bar{t}H$, $t\bar{t}l\bar{l}$, $t\bar{t}l\nu$, $t\bar{t}l\bar{l}q$, and tHq .

column, we check whether the cross section of the process is scaled by more than five times the SM cross section when the WC associated with the operator is set to $16\pi^2$ or $-16\pi^2$ [11]. For the operators that are associated with multiple WCs, if any of the WCs causes the process to be scaled by more than five times the SM cross section, the process is considered to be affected by that operator. The choice to use a factor of five as the criterion for this determination is arbitrary; if it were changed, the list of processes listed in the column would potentially change as well. However, changing these criteria would have no influence on the analysis, as the effects of all operators on all process are fully considered. The diagrams in Fig. 2 illustrate two examples of interactions that arise from one of the operators we consider; these interactions can affect the signal process $t\bar{t}H$.

The signal events are generated using an approach similar to the one described in Ref. [46]. Like the framework presented there, the model used in this analysis adopts the Warsaw basis of gauge-invariant dimension-six operators [9], focuses on operators that give rise to interactions involving at least one top quark, and only allows for tree-level generation. To allow MADGRAPH5_aMC@NLO to properly handle the emission of gluons from O_{uG} vertices, an extra factor of the strong coupling is applied to the coefficients arising from the O_{uG} operator. Since only tree-level generation is possible with this model, the $t\bar{t}H$, $t\bar{t}l\nu$, and $t\bar{t}l\bar{l}$ signal samples are generated with an extra parton in the final state, improving accuracy and allowing some operators to contribute more significantly to processes upon which they would otherwise have

Table 1: List of operators that have effects on $t\bar{t}H$, $t\bar{t}\bar{l}\bar{l}$, $t\bar{t}l\nu$, $t\bar{t}\bar{l}q$, and tHq processes at order $1/\Lambda^2$ that are considered in this analysis. The couplings are assumed to involve only third-generation quarks. The quantity $T^A = \frac{1}{2}\lambda^A$ denotes the eight Gell-Mann matrices, and τ^I are the Pauli matrices. The field φ is the Higgs boson doublet, and $\tilde{\varphi} = \varepsilon\varphi^*$, where $\varepsilon \equiv i\tau^2$. The ℓ and q represent the left-handed lepton and quark doublets, respectively, while e represents the right-handed lepton, and u and d represent the right-handed quark singlets. Furthermore, $(\varphi^\dagger i\overleftrightarrow{D}_\mu \varphi) \equiv \varphi^\dagger(iD_\mu \varphi) - (iD_\mu \varphi^\dagger)\varphi$ and $(\varphi^\dagger i\overleftrightarrow{D}_\mu^I \varphi) \equiv \varphi^\dagger \tau^I(iD_\mu \varphi) - (iD_\mu \varphi^\dagger)\tau^I \varphi$. The W boson field strength is $W_{\mu\nu}^I = \partial_\mu W_\nu^I - \partial_\nu W_\mu^I + g\varepsilon_{IJK}W_\mu^J W_\nu^K$, and $G_{\mu\nu}^A = \partial_\mu G_\nu^A - \partial_\nu G_\mu^A + g_s f^{ABC}G_\mu^B G_\nu^C$ is the gluon field strength. The abbreviations s_W and c_W denote the sine and cosine of the weak mixing angle (in the unitary gauge), respectively. The leading processes affected by the operators are also listed (the details of the criteria used for this determination are described in the text).

Operators involving two quarks and one or more bosons			
Operator	Definition	WC	Lead processes affected
$\dagger O_{u\varphi}^{(ij)}$	$\bar{q}_i u_j \tilde{\varphi} (\varphi^\dagger \varphi)$	$c_{t\varphi} + ic_{t\varphi}^I$	$t\bar{t}H, tHq$
$O_{\varphi q}^{1(ij)}$	$(\varphi^\dagger i\overleftrightarrow{D}_\mu \varphi)(\bar{q}_i \gamma^\mu q_j)$	$c_{\varphi Q}^- + c_{\varphi Q}^3$	$t\bar{t}H, t\bar{t}l\nu, t\bar{t}\bar{l}\bar{l}, tHq, t\bar{l}q$
$O_{\varphi q}^{3(ij)}$	$(\varphi^\dagger i\overleftrightarrow{D}_\mu^I \varphi)(\bar{q}_i \gamma^\mu \tau^I q_j)$	$c_{\varphi Q}^3$	$t\bar{t}H, t\bar{t}l\nu, t\bar{t}\bar{l}\bar{l}, tHq, t\bar{l}q$
$O_{\varphi u}^{(ij)}$	$(\varphi^\dagger i\overleftrightarrow{D}_\mu \varphi)(\bar{u}_i \gamma^\mu u_j)$	$c_{\varphi t}$	$t\bar{t}H, t\bar{t}l\nu, t\bar{t}\bar{l}\bar{l}, t\bar{l}q$
$\dagger O_{\varphi ud}^{(ij)}$	$(\tilde{\varphi}^\dagger iD_\mu \varphi)(\bar{u}_i \gamma^\mu d_j)$	$c_{\varphi tb} + ic_{\varphi tb}^I$	$t\bar{t}H, t\bar{l}q, tHq$
$\dagger O_{uW}^{(ij)}$	$(\bar{q}_i \sigma^{\mu\nu} \tau^I u_j) \tilde{\varphi} W_{\mu\nu}^I$	$c_{tW} + ic_{tW}^I$	$t\bar{t}H, t\bar{t}l\nu, t\bar{t}\bar{l}\bar{l}, tHq, t\bar{l}q$
$\dagger O_{dW}^{(ij)}$	$(\bar{q}_i \sigma^{\mu\nu} \tau^I d_j) \varphi W_{\mu\nu}^I$	$c_{bW} + ic_{bW}^I$	$t\bar{t}H, t\bar{t}\bar{l}\bar{l}, tHq, t\bar{l}q$
$\dagger O_{uB}^{(ij)}$	$(\bar{q}_i \sigma^{\mu\nu} u_j) \tilde{\varphi} B_{\mu\nu}$	$(c_W c_{tW} - c_{tZ})/s_W + i(c_W c_{tW}^I - c_{tZ}^I)/s_W$	$t\bar{t}H, t\bar{t}l\nu, t\bar{t}\bar{l}\bar{l}, tHq, t\bar{l}q$
$\dagger O_{uG}^{(ij)}$	$(\bar{q}_i \sigma^{\mu\nu} T^A u_j) \tilde{\varphi} G_{\mu\nu}^A$	$c_{tG} + ic_{tG}^I$	$t\bar{t}H, t\bar{t}l\nu, t\bar{t}\bar{l}\bar{l}, tHq, t\bar{l}q$
Operators involving two quarks and two leptons			
Operator	Definition	WC	Lead processes affected
$O_{\ell q}^{1(ijkl)}$	$(\bar{\ell}_i \gamma^\mu \ell_j)(\bar{q}_k \gamma^\mu q_\ell)$	$c_{Q\ell}^{-(\ell)} + c_{Q\ell}^{3(\ell)}$	$t\bar{t}l\nu, t\bar{t}\bar{l}\bar{l}, t\bar{l}q$
$O_{\ell q}^{3(ijkl)}$	$(\bar{\ell}_i \gamma^\mu \tau^I \ell_j)(\bar{q}_k \gamma^\mu \tau^I q_\ell)$	$c_{Q\ell}^{3(\ell)}$	$t\bar{t}l\nu, t\bar{t}\bar{l}\bar{l}, t\bar{l}q$
$O_{\ell u}^{(ijkl)}$	$(\bar{\ell}_i \gamma^\mu \ell_j)(\bar{u}_k \gamma^\mu u_\ell)$	$c_{t\ell}^{(\ell)}$	$t\bar{t}\bar{l}\bar{l}$
$O_{e\bar{q}}^{(ijkl)}$	$(\bar{e}_i \gamma^\mu e_j)(\bar{q}_k \gamma^\mu q_\ell)$	$c_{Qe}^{(\ell)}$	$t\bar{t}\bar{l}\bar{l}, t\bar{l}q$
$O_{eu}^{(ijkl)}$	$(\bar{e}_i \gamma^\mu e_j)(\bar{u}_k \gamma^\mu u_\ell)$	$c_{te}^{(\ell)}$	$t\bar{t}\bar{l}\bar{l}$
$\dagger O_{\ell equ}^{1(ijkl)}$	$(\bar{\ell}_i e_j) \varepsilon (\bar{q}_k u_\ell)$	$c_t^{S(\ell)} + ic_t^{SI(\ell)}$	$t\bar{t}\bar{l}\bar{l}, t\bar{l}q$
$\dagger O_{\ell equ}^{3(ijkl)}$	$(\bar{\ell}_i \sigma^{\mu\nu} e_j) \varepsilon (\bar{q}_k \sigma_{\mu\nu} u_\ell)$	$c_t^{T(\ell)} + ic_t^{TI(\ell)}$	$t\bar{t}l\nu, t\bar{t}\bar{l}\bar{l}, t\bar{l}q$

a weaker effect.

For the samples generated with an additional parton, a matching procedure is applied to account for the overlap in phase space between the ME and parton shower (PS) contributions; in this analysis, we use the MLM scheme [33]. Since EFT effects are included in the ME contribution but not in the PS contribution, the validity of the matching procedure must be examined

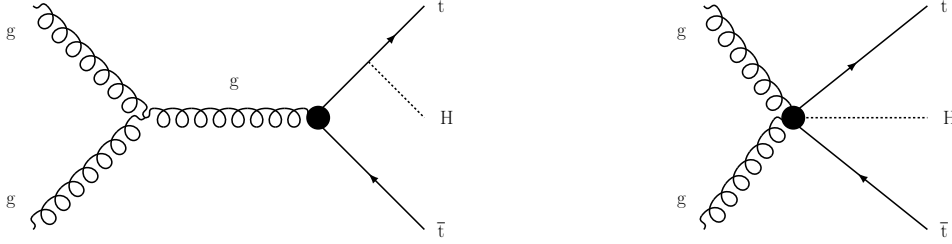


Figure 2: Example diagrams showing two of the vertices associated with the O_{uG} operator. This operator, whose definition can be found in Table 1, gives rise to vertices involving top quarks, gluons, and the Higgs boson; as illustrated here, these interactions can contribute to the $t\bar{t}H$ process.

for operators that give rise to vertices involving a gluon. The only such operator considered by this analysis is O_{uG} , and contributions from this operator to the soft and collinear regime are suppressed; therefore, the phase space overlap with the SM contribution from the PS is small, and the effects of this potential issue are mitigated. The $t\bar{t}q$ and tHq signal samples are not generated with an extra final state parton since, when using the MLM scheme with LO MADGRAPH5_aMC@NLO, jet matching cannot be correctly performed between the ME and the PS for single top quark processes in the t channel.

3.2 Parameterization of the yields in terms of the WCs

In order to discern the effects of new physics on the observed yields, the predicted yields must be parameterized in terms of the WCs. First, the ME can be written as the sum of SM and new physics components:

$$\mathcal{M} = \mathcal{M}_{\text{SM}} + \sum_i \frac{c_i}{\Lambda^2} \mathcal{M}_i, \quad (2)$$

where \mathcal{M}_{SM} is the SM ME, \mathcal{M}_i are the MEs corresponding to the new physics components, and c_i are the WCs. Any cross section—inclusive or differential—is proportional to the square of the ME. The SM contribution to the cross section is necessarily independent of the WC values, while the new EFT operators have contributions that depend linearly on the coefficients arising from the interference with the SM and contributions quadratic in the coefficients from pure EFT terms. The latter can originate from the effects of an individual operator or interference between the EFT operators. Since this analysis considers 16 WCs, the expected cross section could therefore be parameterized as a 16-dimensional (16D) quadratic function of the WCs.

In principle, the 16D quadratic terms could be fully determined by evaluating the cross section at multiple points in WC space and solving for the coefficients; it would be impractical, however, to produce the large number of simulated samples required. Instead, we use the MADGRAPH5_aMC@NLO event generator’s ability to assign weights to the generated events in order to effectively account for the variation of the differential cross section in an infinitesimal part of phase space occupied by an individual event. Each event weight, just like the inclusive or differential cross section, can be parameterized by a polynomial of second order in the WCs. In order to determine the coefficients of each event’s 16D quadratic weight function, the weight is calculated at multiple randomly selected points in the 16D WC phase space. Once enough weights have been calculated to constrain the 16D quadratic function, we can solve for the coefficients and therefore obtain the parameterization for the weight function of each event in terms of the WCs. The weight functions w_i for a given event i can then be written as

follows:

$$w_i \left(\frac{\vec{c}}{\Lambda^2} \right) = s_{0i} + \sum_j s_{1ij} \frac{c_j}{\Lambda^2} + \sum_j s_{2ij} \frac{c_j^2}{\Lambda^4} + \sum_{j,k} s_{3ijk} \frac{c_j}{\Lambda^2} \frac{c_k}{\Lambda^2}, \quad (3)$$

where \vec{c} represents the set of WCs, the sum over j and k corresponds to the sum over the WCs, and the values s_0 , s_1 , s_2 , and s_3 represent the coefficients in the quadratic parameterization of the weight from the SM, interference between EFT and SM, pure EFT, and interference between two EFT contributions, respectively.

The weighted events can then be used to calculate predicted yields for an arbitrary set of WC values; the yield for a given event selection category (as discussed in Section 5) is found by summing the weight functions for events that meet the selection requirements of the given category. Thus, summing Eq. (3) over i , we find the predicted yield N :

$$\begin{aligned} N \left(\frac{\vec{c}}{\Lambda^2} \right) &= \sum_i w_i \left(\frac{\vec{c}}{\Lambda^2} \right) \\ &= \sum_i \left(s_{0i} + \sum_j s_{1ij} \frac{c_j}{\Lambda^2} + \sum_j s_{2ij} \frac{c_j^2}{\Lambda^4} + \sum_{j,k} s_{3ijk} \frac{c_j}{\Lambda^2} \frac{c_k}{\Lambda^2} \right) \\ &= \left(\sum_i s_{0i} \right) + \sum_j \left(\sum_i s_{1ij} \right) \frac{c_j}{\Lambda^2} + \sum_j \left(\sum_i s_{2ij} \right) \frac{c_j^2}{\Lambda^4} + \sum_{j,k} \left(\sum_i s_{3ijk} \right) \frac{c_j}{\Lambda^2} \frac{c_k}{\Lambda^2} \\ &= S_0 + \sum_j S_{1j} \frac{c_j}{\Lambda^2} + \sum_j S_{2j} \frac{c_j^2}{\Lambda^4} + \sum_{j,k} S_{3jk} \frac{c_j}{\Lambda^2} \frac{c_k}{\Lambda^2}. \end{aligned} \quad (4)$$

The predicted yield has therefore been expressed as a quadratic function of the WCs, where the quadratic coefficients of the yield parameterization were found by summing the quadratic coefficients of the weights, e.g., $S_{1j} = \sum_i s_{1ij}$. Since the parameterized yields should be consistent with the SM when all WCs are set to zero, we normalize the yields to the NLO predictions [47].

4 Event reconstruction

The CMS global (also called particle-flow (PF) [48]) event reconstruction aims to reconstruct and identify each individual particle in an event, with an optimized combination of all sub-detector information. In this process, the identification (ID) of the particle type (photon, electron, muon, charged or neutral hadron) plays an important role in the determination of the particle direction and energy. Photons are identified as ECAL energy clusters not linked to the extrapolation of any charged particle trajectory to the ECAL. Electrons are identified as a primary charged particle track and potentially many ECAL energy clusters corresponding to this track extrapolation to the ECAL and to possible bremsstrahlung photons emitted along the way through the tracker material. Muons are identified as tracks in the central tracker consistent with either a track or several hits in the muon system, and associated with calorimeter deposits compatible with the muon hypothesis. Charged hadrons are identified as charged-particle tracks neither identified as electrons, nor as muons. Finally, neutral hadrons are identified as HCAL energy clusters not linked to any charged hadron trajectory, or as a combined ECAL and HCAL energy excess with respect to the expected charged hadron energy deposit.

The energy of photons is obtained from the ECAL measurement. The energy of electrons is determined from a combination of the charged track momentum at the main interaction vertex, the corresponding ECAL cluster energy, and the energy sum of all bremsstrahlung photons

attached to the track. The energy of muons is obtained from the corresponding track momentum. The energy of charged hadrons is determined from a combination of the track momentum and the corresponding ECAL and HCAL energies, corrected for the response function of the calorimeters to hadronic showers. Finally, the energy of neutral hadrons is obtained from the corresponding corrected ECAL and HCAL energies.

The missing transverse momentum vector (\vec{p}_T^{miss}) is computed as the negative vector sum of the transverse momenta of all the PF candidates in an event, and its magnitude is denoted as p_T^{miss} [49]. The vector \vec{p}_T^{miss} is modified to account for corrections to the energy scale of the reconstructed jets in the event.

The candidate vertex with the largest value of the sum of squared physics-object transverse momentum (p_T) is taken to be the primary pp interaction vertex. The physics objects are the jets, clustered using the anti- k_T jet finding algorithm [50, 51] with the tracks assigned to the vertex as inputs, and the associated \vec{p}_T^{miss} . More details are given in Section 9.4.1 of Ref. [52]. Lepton candidates, which are subsequently reconstructed, are required to be compatible with originating from the selected primary vertex.

Electrons are reconstructed by matching tracks in the silicon tracker to the energy deposit in the ECAL, without any significant energy deposit in the HCAL [53]. Genuine electrons are distinguished from hadrons mimicking an electron signature by a multivariate algorithm using the quality of the electron track, the shape of the electron cluster, and the matching between the track momentum and direction with the sum and position of energy deposits in the ECAL. Furthermore, to reject electrons produced in photon conversions, candidates with missing hits in the innermost tracking layers or matched to a conversion secondary vertex are discarded.

Muon candidates are reconstructed by combining information from the silicon tracker and the outer muon spectrometer of CMS in a global fit [54]. The quality of the geometrical matching between the individual measurements in the tracker and the muon system is used to improve the ID of genuine prompt muons by substantially reducing misidentification due to hadrons punching through the calorimeters or from muons produced through in-flight decays of kaons and pions.

The electron and muon selection criteria described above define the “loose” lepton selection. Additional selection criteria are applied to discriminate leptons produced in the decays of W and Z bosons and τ leptons from leptons produced in the decays of b or light hadrons, or from misidentified jets. We will refer to the former as “prompt” leptons and to the latter as “nonprompt” leptons. Isolation criteria are also applied to all leptons.

A multivariate analysis (MVA) approach based on boosted decision trees (BDTs), referred to as the prompt lepton MVA, is used for this selection. Each BDT takes as inputs the lepton kinematic, ID, and impact parameter information, as well as kinematic and b tagging information about the nearest jet to the lepton. Two versions of the lepton MVA are trained, one for electrons and one for muons, which differ based on the inclusion of one additional observable for each of the two versions. For electrons, the extra input is the multivariate discriminant developed via dedicated analysis for electron ID [53]. For muons, the extra input is a similar discriminant that classifies the compatibility of track segments in the muon system with the pattern expected from a muon ionization [55]. The BDT inputs have been checked in control regions in data to ensure that they are well modeled by the simulation. A more detailed description of the lepton MVA can be found in [56].

In the signal region, lepton candidates are required to exceed a given discriminant threshold, referred to as the “tight” lepton selection. A looser selection, referred to as the “relaxed” selec-

tion, is defined by relaxing the above lepton MVA discriminant requirement for the purpose of estimating background processes, as discussed in Section 6. The efficiency of the triggers based on the presence of one, two, or three electrons or muons is measured in data in $Z/\gamma^* \rightarrow ee$ and $Z/\gamma^* \rightarrow \mu\mu$ events, respectively. These events are also used to measure the efficiency for electrons or muons to pass the lepton reconstruction, ID, and isolation criteria [53, 54].

For each event, hadronic jets are clustered from PF candidates using the anti- k_T algorithm with a distance parameter of 0.4. Jet momentum is determined as the vectorial sum of all particle momenta in the jet, and is found from simulation to be, on average, within 5 to 10% of the true momentum over the whole p_T spectrum and detector acceptance. Pileup can contribute additional tracks and calorimetric energy depositions to the jet momentum. To mitigate this effect, charged particles originating from pileup vertices are discarded and an offset correction is applied to account for the remaining contributions. Jet energy corrections are derived from simulation to bring measured response of jets to that of particle level jets on an average. In situ measurements of the momentum balance in dijet, photon+jet, Z+jets, and multijet events are used to account for any residual differences in jet energy scale in data and simulation [57]. The jet energy resolution amounts typically to 15–20% at 30 GeV, 10% at 100 GeV, and 5% at 1 TeV [57]. Jets are rejected if the distance in η - ϕ space (where the ϕ is azimuthal angle in radians) between the jet and the closest lepton is less than 0.4.

Jets originating from the hadronization of b quarks are identified by two “combined secondary vertex” algorithms [58, 59], namely CSVv2 and DeepCSV, which exploit observables related to the long lifetime of b hadrons and to the higher particle multiplicity and mass of b jets compared to light-quark and gluon jets. DeepCSV is used for b jet selection, while CSVv2 is used to aid lepton ID as an input to the prompt lepton MVA. The analysis uses two levels of selection based on DeepCSV, with a loose and a medium working point. The medium (loose) working point has approximately 70 (85)% efficiency for tagging jets from b quarks, with a misidentification probability of 1.0(10)% for light quark and gluon jets [59].

5 Event selection

The goal of the event selection is to retain $t\bar{t}H$, $t\bar{t}l\nu$, $t\bar{t}l\bar{l}$, $t\bar{t}lq$, and tHq events while excluding as many contributions from background processes as possible. The analysis is split into categories with two same-sign leptons ($2\ell ss$), three leptons (3ℓ), and four leptons (4ℓ), where ℓ refers to either a e or μ . Events must also have a minimum number of jets, as well as b jets, with additional requirements that depend on the lepton flavor and multiplicity. Single- and double-lepton triggers are used to collect events containing two leptons. For events with three or more leptons, a combination of single-, double-, and triple-lepton triggers are used.

All events are required to have at least two leptons passing the tight selection. Events where a pair of tight leptons with an invariant mass less than 12 GeV is found are rejected, to avoid backgrounds from light resonances. In addition, events must have at least two jets with $p_T > 30$ GeV to be reconstructed in the pseudorapidity (η) region, $|\eta| < 2.4$. One or more of the jets also need to pass the medium working point of the DeepCSV b tagging algorithm, as at least one top quark whose decay produces a bottom quark jet is present in all signal events. No explicit identification requirements are placed on τ leptons, which are allowed to enter the event selection via their decay products.

5.1 $2\ell ss$ category

The $2\ell ss$ category primarily targets $t\bar{t}H$ and $t\bar{t}l\nu$ signal events in which the $t\bar{t}$ system decays semileptonically, with an additional, identically charged lepton coming from the decay of a W boson produced in association with a top quark pair (in the case of $t\bar{t}l\nu$), or coming from the decay of a W boson or a τ lepton produced in the decay of the Higgs boson (in the case of $t\bar{t}H$). In addition, the $t\bar{t}l\bar{l}$ process may contribute with events in which there is at least one lepton that is not reconstructed or does not pass the selection. Selected events are required to contain exactly two same-sign leptons passing the tight criteria, with the lepton of higher (lower) p_T required to have $p_T > 25$ (15) GeV. Residual $t\bar{t}+jets$ background contributions are suppressed by requiring that the charge of all electrons and muons, which pass the relaxed object selection criteria, is well measured. Electrons are required to pass two conditions which test the consistency between the independent measurements of the electron charge obtained from the position of the ECAL cluster and from its track, while muons must satisfy the condition that the estimated uncertainty on the p_T of the muon track is below 20%. The events are required to contain at least four jets with $p_T > 30$ GeV and $|\eta| < 2.4$. At least two of these jets must be b jets, one of which must satisfy the medium working point of the DeepCSV b tagging algorithm, while the second is allowed to pass the loose working point. Events containing more than two tight leptons are vetoed to avoid overlap with the 3ℓ and 4ℓ categories.

5.2 3ℓ category

The 3ℓ category selects $t\bar{t}l\nu$ events in which all three W bosons decay leptonically; $t\bar{t}l\bar{l}$ events in which the $t\bar{t}$ system decays semileptonically and the Z boson decays to two charged leptons; $t\bar{t}lq$ events in which the top quark decays leptonically and the Z decays to two charged leptons; and $t\bar{t}H$ events in which the H decays to W , Z or τ particles, at least one of which then decays leptonically (with one or more charged leptons also coming from the decay of the $t\bar{t}$ system). Selected events are required to contain exactly three charged leptons passing the tight object selection criteria. The three charged leptons are required to have $p_T > 25$, 15, and 10 GeV. In the case that the third lepton is an electron, the requirement on it is instead $p_T > 15$ GeV in order to stay above the trigger thresholds and keep the contributions from nonprompt electrons under control. Two or more jets with $p_T > 30$ GeV and $|\eta| < 2.4$ are required, at least one of which must satisfy the medium working point of the DeepCSV b tag algorithm. Two subcategories are defined according to whether a second jet passing the medium b tag is present. This avoids incorrectly promoting $t\bar{t}lq$ events into the subcategory requiring two b jets, due to misidentification.

5.3 4ℓ category

The 4ℓ category targets $t\bar{t}l\bar{l}$ events in which all the W and Z bosons decay leptonically, and $t\bar{t}H$ events in which the H decays into a pair of W bosons, where all W bosons decay leptonically; Z bosons, where at least one Z decays leptonically; or leptonically decaying τ leptons. Events selected in this category are required to contain four or more leptons passing the tight object selection criteria and passing p_T thresholds of $p_T > 25$, 15, 10, and 10 GeV for the lepton of highest, second, third, and fourth highest p_T , respectively. In the case of electrons, the requirement on the third or fourth lepton is instead $p_T > 15$ GeV for the same reasons as in the 3ℓ category. Two or more jets with $p_T > 30$ GeV and $|\eta| < 2.4$ are required. As in the $2\ell ss$ category, at least two of these jets must be b jets, one of which must satisfy the medium working point of the DeepCSV b tagging algorithm, while the second is allowed to pass the loose working point.

Table 2: Requirements for the different event categories. Requirements separated by commas indicate a division into subcategories. The b jet requirement on individual jets varies based on the lepton category, as described in the text.

Selection	$2\ell ss$	3ℓ		$\geq 4\ell$
Leptons	Exactly 2 leptons	Exactly 3 leptons		≥ 4 leptons
Charge requirements	$\sum_{\ell} q < 0, \sum_{\ell} q > 0$	$\sum_{\ell} q < 0, \sum_{\ell} q > 0$	—	—
Jet multiplicity	4, 5, 6, ≥ 7 jets	2, 3, 4, ≥ 5 jets	2, 3, 4, ≥ 5 jets	2, 3, ≥ 4 jets
Number of b jets	≥ 2 b jets	1, ≥ 2 b jets	1, ≥ 2 b jets	≥ 2 b jets
Dilepton mass	—	$ m_{\ell\ell} - m_Z > 10 \text{ GeV}$	$ m_{\ell\ell} - m_Z \leq 10 \text{ GeV}$	—

5.4 Separation into subcategories

Events in the $2\ell ss$, 3ℓ , and 4ℓ categories are further separated based on a number of criteria, as summarized in Table 2. In the $2\ell ss$ category, events are further separated based on lepton charge. This allows us to take advantage of the fact that the $t\bar{t}W^+$ cross section is roughly a factor of 2 larger than that of the $t\bar{t}W^-$ cross section, so it is enhanced in $2\ell ss$ events where both leptons are positively charged. In the 3ℓ category, we consider separately events which contain a same-flavor, oppositely charged pair of leptons with an invariant mass that falls within 10 GeV of the m_Z , which primarily serves to create a region where the contribution from (on-shell) $t\bar{t}Z$ is enhanced. For 3ℓ events that do not fall within this region, a classification based on the sum of lepton charges is used, considering events where the charge sum is positive separately from those where it is negative. This again exploits the difference in cross section between $t\bar{t}W^+$ and $t\bar{t}W^-$. In all 3ℓ events, a classification is done based on whether the event contains exactly one jet passing the medium DeepCSV working point, or two or more jets passing the medium DeepCSV working point; the contribution from $t\bar{t}l\bar{l}q$ is enhanced in the former case. For the 4ℓ category, events are not split based on the invariant dilepton mass due to a small population of events in those bins.

Events in all categories are then separated into jet-multiplicity bins, which are used to fit to data and place limits on EFT parameters, as described in Section 7. The $2\ell ss$ and 3ℓ categories are split into four jet multiplicity bins, resulting in 8 and 24 subcategories respectively. The 4ℓ category is split into three jet bins, bringing the total to 35 distinct signal region subcategories.

6 Background estimation

Contributions to the selected event yields arise from a variety of background processes, which can be categorized as reducible or irreducible and are either estimated from data control regions or modeled using simulation. A background is considered as reducible in case one or more of the reconstructed electrons or muons passing the tight object selection are not due to genuine prompt leptons, as defined in Section 4.

In the $2\ell ss$ categories, a reducible background arises from events containing lepton pairs of opposite charge, mostly from $t\bar{t}$ +jets production, in which the charge of one lepton is mismeasured. Both background contributions are determined from data using the same methods as in Ref. [56]. A summary of these procedures is given in Sections 6.1 and 6.2.

The dominant irreducible background processes are diboson production and (to a lesser extent) triboson production and are estimated using simulations. In the 3ℓ and 4ℓ categories in particular, diboson production is the dominant overall background (among both reducible and irreducible sources).

The production of a top quark pair in association with a photon represents an additional, minor

source of background. It is typically due to an asymmetric photon conversion into an electron-positron pair, where one of the produced particles carries most of the photon energy while the other one is not reconstructed. Even though this is a reducible background source, its contribution is estimated using simulation, since the isolated leptons arising from asymmetric conversion are well described in simulation.

6.1 Background from misidentified leptons

The background from nonprompt leptons is estimated from control samples in data, applying the measured rate at which nonprompt leptons pass the lepton selection criteria. This rate, referred to as the fake rate, is measured from a multijet sample dominated by nonprompt leptons. The data analyzed in this region are collected with single lepton triggers, except at low muon p_T , where the presence of an additional jet with $p_T > 40$ GeV is required in the trigger. The misidentification rate is defined as the probability for a lepton candidate that passes a relaxed lepton cut to pass the tight lepton selection. The misidentification rate is extracted separately for electrons and muons and is measured as a function of the p_T and η of the nonprompt lepton. Contamination from prompt leptons in the multijet sample is subtracted based on expectations from simulation.

Once the misidentification rates have been determined, they are applied to a selection called the application region (AR), which is identical to the signal region except that one or more of the leptons are required to fail the tight selection but pass the relaxed lepton selection instead. An estimate of the misidentified-lepton background in the SR is obtained by applying appropriately chosen weights to the events selected in the AR. Further details on the nonprompt-lepton background estimation technique can be found in Ref. [56].

6.2 Background from lepton charge mismeasurement

The lepton charge mismeasurement background in the $2\ell ss$ categories is dominated by $t\bar{t}$ events with two prompt leptons in which the sign of either prompt lepton is mismeasured. This background contribution is estimated from data, following a strategy similar to the one used for the estimation of the nonprompt background. It is found to be relevant only for electrons. The electron charge is defined using the majority method, which takes the charge to be the one shared by at least two of the three charge estimate methods [53]. An AR is defined for the $2\ell ss$ categories, requiring that the two selected leptons are of opposite charge. The events in the AR are then weighted using the probability to mismeasure the electron charge, derived in a $Z/\gamma^* \rightarrow ee$ sample and parameterized as a function of the electron p_T and η . The probability for mismeasuring the sign of electrons ranges from 0.02% for electrons in the barrel to 0.2% for electrons in the endcaps, after all the object selection criteria. The sum of the charge mismeasurement probabilities of the two lepton candidates is used to determine the overall background.

7 Signal extraction

As stated in Section 5.4, the analysis is split into 35 statistically independent categories, based on the sum of lepton charges, number of b tagged jets, and jet multiplicity. A likelihood function is built based on independent bins following Poisson statistics. The event yields are a function of the WCs and a set of nuisance parameters (NPs) which contain the effects of systematic uncertainties (see Section 8). The WCs are parameterized by the quadratic form for the cross section as explained in Section 3. In order to fit this parameterization to the data, we scan over all WCs. The boundaries of the scans roughly correspond to values of the chosen operator

that result in a five-fold increase in the SM cross section for at least one signal process. At each point in the scan, the negative log profiled-likelihood is computed, and the best fit is evaluated as the WC which minimizes the negative log likelihood. Confidence intervals of 1 and 2 standard deviations (σ) are calculated by finding where the negative log likelihood curve crosses twice the value of one and four respectively. In principle, this scan can be performed in the 16D WC space. However, fitting this hypersurface is time-consuming, and the results are difficult to interpret. Instead, we perform the fit for a single WC in two scenarios: when the other 15 WCs are treated as unconstrained NPs (profiled); and when the other 15 WCs are fixed to their SM value of zero.

8 Systematic uncertainties

There are two types of systematic effects considered: those that affect only the rates of signal or background processes, and those that affect both the rate and the shape which refers to changes in the relative expected yield of the jet and/or b jet bins. In the latter case, the rate and shape effects are treated simultaneously so that they are considered fully correlated. Each systematic uncertainty is correlated across all analysis bins by using a single NP per physical process. The sources of systematic uncertainties considered are: the integrated luminosity; the jet energy scale (JES); b jet tagging scale factors; the theoretical cross section; the PDF shape variations; the renormalization (μ_R) and factorization (μ_F) scales; the PS; the parton matching; the additional radiation; the muon and electron ID, isolation, trigger efficiency; the pileup; the misidentified-lepton rate estimate; and the charge misreconstruction estimate.

All variations listed are applied equally to the signal and background samples, and are treated as 100% correlated across all samples. Unless otherwise stated, all systematic uncertainties are considered independent and thus uncorrelated with each other.

- *Integrated luminosity* The measured uncertainty on the LHC integrated luminosity estimate is 2.3% [30].
- *Jet Energy Scale* The JES is adjusted via scale factors to account for pileup, nonuniform detector response, and any residual differences between the data and simulation. The resulting effect of the JES uncertainty on the yields is determined by shifting the jet energy correction up and down by 1σ , and propagating the changes through the object ID and event selection.
- *b jet tagging scale factors* In order to use the DeepCSV tagger for identifying b jets, scale factors are applied to the simulated samples to bring them in agreement with data [59]. There are three types of systematic uncertainties associated with the use of these scale factors: the JES, the purity of the control samples used to derive the scale factors, and the size of all the samples used to derive the scale factors. The JES dependence is calculated simultaneously with the JES systematic uncertainty. The purity component is treated by assigning NPs for the yields from both the light (g, u, d, s) and heavy (c, b) flavors. The c jet tagging uncertainty is used to remove c jets potentially mistagged as b jets. Finally, the statistical uncertainty of the samples used to derive the scale factors is taken into account with four NPs: two for the light-flavor (LF) case and two for the heavy-flavor (HF) case. The two NPs for each case are: an NP for the overall tilt that would be consistent with the statistical uncertainties on the SFs, while the second NP controls distortions of a more complicated nature, where the upper and lower ends of the distribution change relative to the center. These NPs account for discrepancies in the shape of the tagging discriminant distributions, which are consistent with the uncertainty of the scale factors.

Table 3: Cross section (rate) uncertainties used for the fit. Each column in the table is an independent source of uncertainty. Uncertainties in the same column for different processes (different rows) are fully correlated.

Process	μ_R and μ_F scales	PDF
$t\bar{t}H$	-9.2% +5.8%	$\pm 3.6\%$
$t\bar{t}l\bar{q}$	$\pm 1\%$	$\pm 4\%$
$t\bar{t}l\nu$	-12% +13%	$\pm 2\%$
$t\bar{t}l\bar{l}$	-12% +10%	$\pm 3\%$
tHq	-8% +6%	$\pm 3.7\%$
Diboson	$\pm 2\%$	$\pm 2\%$
Triboson	$\pm 2.6\%$	$\pm 4.2\%$
$t\bar{t}\gamma$ +jets	$\pm 10\%$	$\pm 5\%$

- *Theoretical cross section* The expected yields for signal and background are derived from theoretical predictions of at least NLO accuracy. There are associated uncertainties on the μ_R and μ_F scales of the process and the PDF. Table 3 summarizes these uncertainties. For signal processes, this uncertainty is considered on the whole process (SM+EFT). These uncertainties do not vary with the WCs, so the uncertainties are of the same magnitude as when fixing the model to the SM component alone.
- *PDF shape variations* The shape variation of the final fitting variable distributions due to the uncertainty on the PDF is estimated by reweighting the spectra according to 100 replica sets. The total uncertainty is measured using the standard PDF4LHC [60] recommendation.
- *Renormalization and factorization scales* Uncertainties due to the μ_R and μ_F scales in the $t\bar{t}$ ME generator are modeled by varying the scales independently by a factor of 1/2 or 2 and propagating the changes to the final fitting variable distribution in the fit. An uncertainty envelope is then calculated from these two systematic uncertainties. This is accommodated via weights obtained directly from the generator information. Since the normalization uncertainties of the ME generators are covered by the cross section uncertainties (listed in Table 3), only the impact on the kinematic shape of the process in question are considered. These shape effects primarily enter as changes in the acceptance and efficiency for events to fall into a particular event selection category. The bounds of the envelope are determined by taking the maximum of the μ_F uncertainties, the μ_R uncertainties, and their sum. The μ_R and μ_F effects on the WCs range between 1 and 5% depending on the bin.
- *Parton shower* The uncertainty in the PS simulation is estimated by varying the μ_R for initial- and final-state radiation (ISR/FSR) up and down in PYTHIA by multiplying/dividing the scale by a factor of 2 for ISR and $\sqrt{2}$ for FSR. A dedicated SM sample (produced without EFT effects) is used to determine this systematic variation; the values obtained through this study are then applied to the full analysis samples.
- *Parton matching* This uncertainty only applies to $t\bar{t}H$, $t\bar{t}W$, and $t\bar{t}Z$ processes, since matching is only performed for processes that include an extra parton. Determined by varying the matching scale value between the extra partons generated in MADGRAPH5_AMC@NLO and jets produced in PYTHIA, this uncertainty is computed bin-by-bin. A dedicated SM sample (produced without any EFT effects) was used to perform this study. The nominal scale is 19 GeV, and is shifted up to 25 GeV and down to 15 GeV.

- *Additional radiation* Since an extra final-state parton was not included in the LO single top quark processes ($t\bar{l}q$ and tHq), they are not expected to be as sensitive to varying the WCs as the LO $t\bar{t}H$, $t\bar{t}W$, and $t\bar{t}Z$ samples. A comparison of the LO $t\bar{l}q$ sample to the NLO tZq sample, reveals a discrepancy in the event yield, which is not covered by the existing systematic uncertainties. We therefore introduced a new systematic uncertainty specifically for the $t\bar{l}q$ sample to cover this disagreement. The same systematic uncertainty is applied to tHq , since the uncertainty accounts for the fact that MADGRAPH5_aMC@NLO cannot handle the matching for these extra partons for any t -channel process. These uncertainties are typically around 20%, but can reach as high as 80% for the high jet multiplicity bins with few events.
- *Muon and electron ID and isolation* Scale factors are used to correct the tracking efficiency, electron and muon ID efficiency, and isolation in the simulation to match that in data, which are derived with a “tag-and-probe” method [53, 54, 61]. The impacts of these quantities are estimated by varying the scale factors within their uncertainties. The resulting systematic uncertainties are typically of the order of 1–2% per lepton.
- *Trigger efficiency* The impact due to the trigger efficiency [54] is estimated by varying the trigger scale factors within their uncertainties, which are in the range of 2–5%.
- *Pileup* Effects due to the uncertainty in the distribution of the number of pileup interactions are evaluated by varying the total inelastic pp cross section used to predict the number of pileup interactions in the simulation by 4.6% from its nominal value, which corresponds to a 1σ variation [62]. This effect typically ranges from less than 1–3%.
- *Misidentified-lepton rate estimate* Several sources of systematic uncertainty are considered. The measurement of the misidentified-lepton weights is affected by the small population in the measurement region, subtraction of prompt lepton contamination in this region, as well as the uncertainty in the background jet composition in this region (dominated by multijet background) and the AR (dominated by $t\bar{t}$ -jets background). The effect on the misidentified lepton rate due to the overall uncertainty of the misidentified leptons is taken into account by varying the entire map of misidentified lepton weights up or down by 1σ . This is the largest source of uncertainty on the misidentified lepton rate, and amounts to approximately 25–30%, depending on the jet multiplicity bin. In addition, the limited population in the AR of the misidentified lepton method have a significant effect on the estimate of the misidentified lepton rate and must be considered as a separate source of uncertainty. This again varies with jet multiplicity bin, and amounts to approximately 10–30%.
- *Charge misidentification probability* The yield of the misreconstructed background in the $2\ell ss$ categories is known with an uncertainty of 30%, and is included as a rate systematic uncertainty. The uncertainty due to the limited population in the corresponding AR is negligible and is not considered.

Table 4 summarizes the systematic uncertainties assessed in the signal and backgrounds, and how each systematic uncertainty is treated in the fit used to extract the amount of signal present in the data sample. We note that it is possible for the statistical and systematic uncertainties to depend on the choice of the initial WC values (used to evaluate the quadratic fit parameters). To examine this, simulations are generated at the boundaries of the measured 2σ confidence interval, and the SM point (i.e., all WCs set to zero), and no difference is observed within the current level of precision. A summary of the percentage effect (change in WC divided by the

symmetrized confidence interval) for c_{tW} , $c_{t\phi}$, $c_{Q\ell}^{-(\ell)}$, and $c_{t\ell}^{(\ell)}$ is provided in the last four columns of Table 4 to illustrate the range of values we observe for each systematic variation. This table is related to the change in the WCs do to a single NP—correlations among NPs are not taken into account—and is therefore a conservative estimate.

9 Results

The number of events selected in different categories is compared to the expected contributions of the signal processes and of the different background processes before (prefit) and after simultaneously fitting all 16 WCs, and the NPs, to minimize the negative log-likelihood (post-fit) in Fig. 3. The prefit scenario corresponds to the SM where the values of the WCs are all assumed to be zero. The simultaneous fit is equivalent to the 16 best fit points from the profiled fits: the profiled fit will always find the global minimum for each of the 15 profiled WCs. The large increase in the tHq event yields is a consequence of the low sensitivity to this particular process coupled with the fact that tHq receives relatively large enhancements from the EFT operators considered. The fit finds a combination of WCs that is able to enhance tHq, which helps improve agreement in the $2\ell ss$ and 3ℓ (non-Z) categories, without spoiling the agreement elsewhere. Despite the large increase, tHq is still a smaller contribution than $t\bar{t}H$ and $t\bar{t}\nu$ in these categories. There is also a large increase in the $t\bar{t}l\bar{q}$ event yields, which we are also insensitive to.

Table 5 shows the 2σ confidence intervals for each WC. Intervals are given for two scenarios. These results are displayed graphically in Fig. 4, along with their 1σ confidence intervals (thicker lines). The confidence intervals for a single WC (solid bars) are calculated while the other 15 WCs are profiled. An alternative determination of the confidence interval for a single WC is performed by fixing the other 15 WCs to their SM values of zero (dashed bars). For the profiled scenario, the confidence interval for all WCs includes the SM. Occasionally, when fixing the other 15 WCs to zero the SM point falls just outside the 2σ confidence interval (e.g., c_{tW}). This is not surprising because in the cases where all WCs but one are fixed to zero, that single WC must account entirely for any deviation between observed data and expectation. In contrast, in the profiled case, all 16 WCs can work together to accommodate any deviations, resulting in a best fit point that is closer to the SM, leading to the SM point falling inside the 2σ confidence interval. It is also sometimes possible for the profiled case to produce a more narrow 2σ confidence interval, as can be seen for $c_t^{S(\ell)}$, $c_{te}^{(\ell)}$, $c_{t\ell}^{(\ell)}$, $c_{Qe}^{(\ell)}$, and $c_{Q\ell}^{-(\ell)}$. It is important to note that these five parameters each have disjoint nonzero 1σ confidence interval when the other 15 parameters are frozen. This will inherently broaden the profiled likelihood curve, resulting in a larger interval.

Additional validation of the results was done with simultaneous scans in two WCs. These are illustrated in Figs. 5–10. This subset of figures are the only ones which show clear signs of correlations between pairs of WCs. The diamond marker corresponds to the SM theoretical prediction. The contours correspond to the 1σ (solid lines), 2σ (thick dashed lines), and 3σ (dash-dotted lines) confidence intervals. Figure 5 indicates minimal correlation between the WCs $c_{Q\ell}^{-(\ell)}$ and $c_{Qe}^{(\ell)}$. This is a common case for many coefficient pairs, especially when the other 14 are profiled. The left panel of Fig. 6 shows a more rectangular contour for $c_{\phi tb}$ and $c_{Q\ell}^{3(\ell)}$. This indicates that these two WCs are not correlated, and the rectangular shape comes from a double minima in $c_{Q\ell}^{3(\ell)}$. Comparing the left and right panels of Fig. 6 shows $c_{Q\ell}^{3(\ell)}$ has little preference over profiling the other 14 WCs versus fixing them to zero, while the $c_{\phi tb}$ range is cut almost in half when fixing the other 14 coefficients to zero. Figure 7 shows a similar behavior for

Table 4: Summary for the systematic uncertainties. Here “shape” means that the systematic uncertainty causes a change in the relative expected yield of the jet and/or b jet bins. Except where noted, each row in this table will be treated as a single, independent NP. Impacts of various systematic variations on a subset of WCs are also quoted. Percentages represent the change in a WC divided by the symmetrized 2σ confidence interval. A value of 100% indicates the particular systematic variation adds an uncertainty equal to the WC interval. The percentages for the b and c jet tags are the sum of all their respective subcategories.

Source	Type	c_{tW}	$c_{t\phi}$	$c_{Q\ell}^{-(\ell)}$	$c_{t\ell}^{(\ell)}$
Integrated luminosity	rate	6%	2%	1%	<1%
JES	rate+shape	6%	2%	1%	<1%
b jet tag		1%	5%	8%	<1%
b jet tag HF fraction	rate+shape				
b jet tag HF stats (linear)	rate+shape				
b jet tag HF stats (quadratic)	rate+shape				
b jet tag LF fraction	rate+shape				
b jet tag LF stats (linear)	rate+shape				
b jet tag LF stats (quadratic)	rate+shape				
c jet mistag		<1%	12%	8%	2%
b jet tag charm (linear)	rate+shape				
b jet tag charm (quadratic)	rate+shape				
PDF (gg)	rate	1%	<1%	<1%	<1%
PDF (gg $_{t\bar{t}H}$)	rate	<1%	1%	<1%	<1%
PDF (q \bar{q})	rate	1%	<1%	<1%	<1%
PDF (qg $_{tHq}$)	rate	<1%	<1%	<1%	<1%
$\mu_{R,F}$ scale (t $\bar{t}H$)	rate	2%	5%	<1%	<1%
$\mu_{R,F}$ scale (t $\bar{t}\gamma$)	rate	1%	1%	<1%	<1%
$\mu_{R,F}$ scale (t $\bar{t}V$)	rate	15%	4%	1%	<1%
$\mu_{R,F}$ scale (tHq)	rate	1%	1%	<1%	<1%
$\mu_{R,F}$ scale (V)	rate	<1%	<1%	<1%	<1%
$\mu_{R,F}$ scale (VV)	rate	<1%	<1%	<1%	<1%
$\mu_{R,F}$ scale (VVV)	rate	<1%	<1%	<1%	<1%
PDF	shape	2%	1%	<1%	<1%
$\mu_{R,F}$ scales	shape	<1%	6%	1%	<1%
FSR	rate+shape	1%	11%	7%	2%
ISR	rate+shape	<1%	8%	3%	<1%
Parton matching	rate+shape	1%	10%	5%	1%
Additional radiation	rate+shape	11%	3%	1%	<1%
Lepton ident./isol.	rate+shape	4%	2%	<1%	<1%
Trigger efficiency	rate+shape	2%	1%	<1%	1%
Pileup	rate+shape	1%	1%	<1%	<1%
Lepton misident.	rate+shape	2%	70%	29%	<1%
Lepton misident. (stat)	rate+shape				
Charge misident.	rate	3%	2%	<1%	<1%

$c_{\phi Q}^3$ and c_{bW} . The right panels of Figs. 8 and 9 show cases where fixing the other 14 WCs to zero prevents the 2D scan from achieving a 1σ confidence interval contour. The right panel

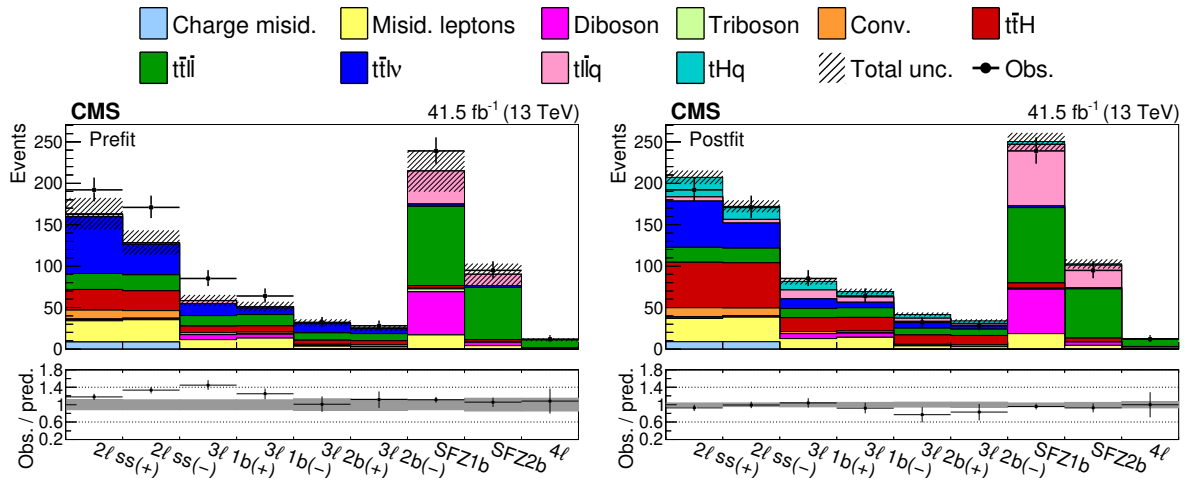


Figure 3: Expected yields prefit (left) and postfit (right). The postfit values of the WCs are obtained from performing the fit over all WCs simultaneously. “Conv.” refers to the photon conversion background, “Charge misid.” is the lepton charge mismeasurement background, and “Misid. leptons” is the background from misidentified leptons. The jet multiplicity bins have been combined here, however, the fit is performed using all 35 event categories outlined in Section 5.4. The lower panel is the ratio of the observation over the prediction.

of Fig. 10 shows a preference in c_{tW} and c_{tZ} for nonzero values when the other 14 WCs are fixed to zero. When the other 14 WCs are profiled (Fig. 10 left), the preference vanishes. This is indicative of the complex interplay between all 16 WCs. Exploring the 16D hypersurface provides a unique handle on the WCs, which was not previously utilized in single parameter analyses such as [16, 19–27]. As a result, any differences compared to other analyses should not be surprising, and may indicate our robust technique more accurately captures the nuances of the EFT.

Figure 11 shows the fractional variation in expected yields for a given process and category after the fit and relative to the SM expectation. The nominal points correspond to the best fit values obtained from the simultaneous fit of all WCs and are therefore the same in each plot. The vertical bars represent the maximum variation in the expected yield within the corresponding 2σ confidence interval for the given WC. The variations are found by profiling all other WCs and NPs, that is by re-running the simultaneous fit for the other WCs and NPs, at each point in the scan for the WC of interest. As the quadratic parameterization for a given WC need not be the same for each process or for each bin of a given process, the extrema of the vertical bars do not necessarily correspond to the same WC values; furthermore, the edges of the vertical bars need not correspond to the 2σ limits of the WC in question. The value for $t\bar{t}lq$ in the 4ℓ category is shown off-scale to preserve the legibility for the rest of the plot. Despite the large ratio, the expected yield in this category is still exceptionally small after the fit and has a negligible contribution to the 2σ confidence intervals.

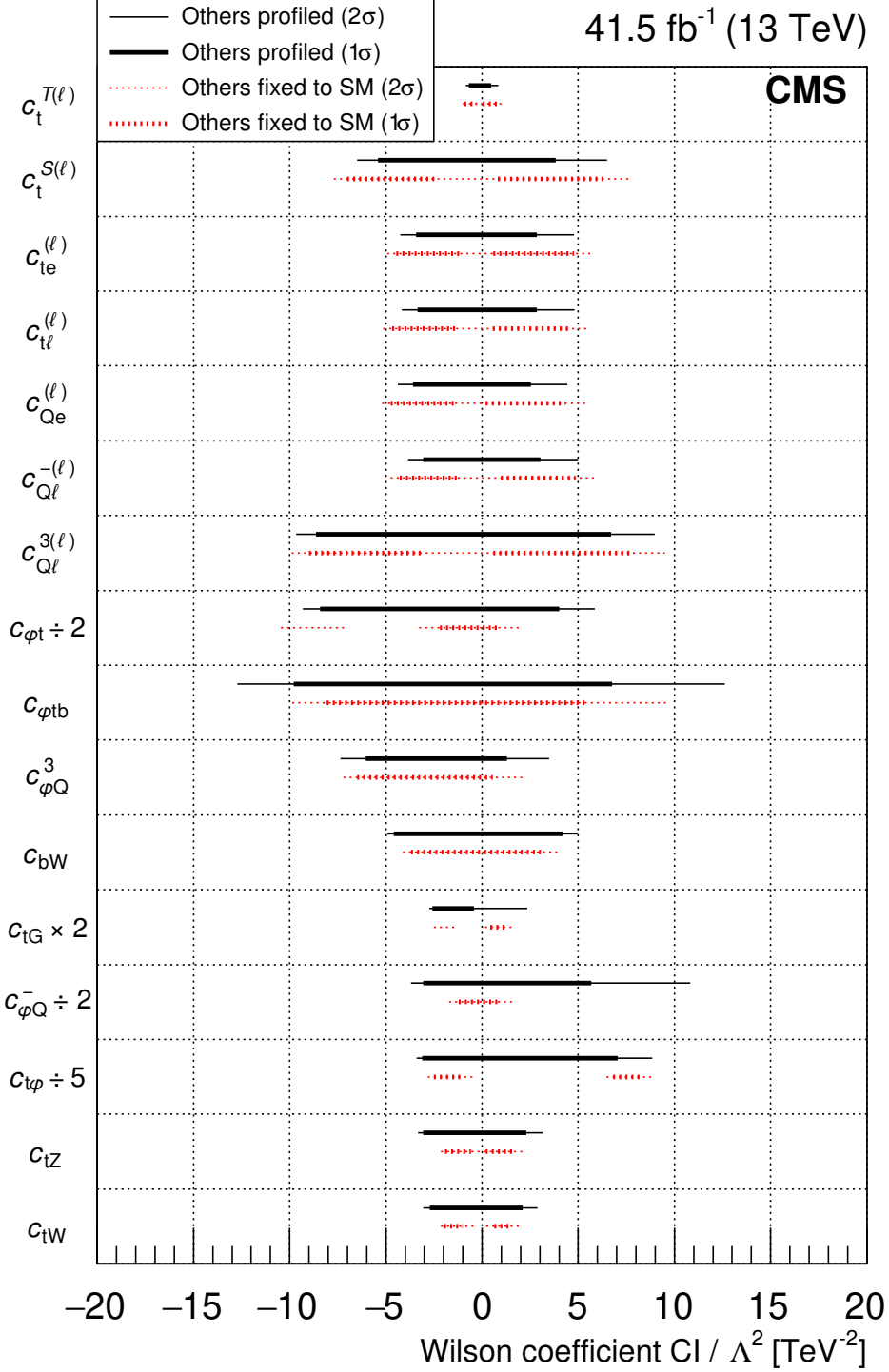


Figure 4: Observed WC 1 σ (thick line) and 2 σ (thin line) confidence intervals (CIs). Solid lines correspond to the other WCs profiled, while dashed lines correspond to the other WCs fixed to the SM value of zero. In order to make the figure more readable, the $c_{\phi t}$ interval is scaled by 1/2, the c_{tG} interval is scaled by 2, the $c_{\phi Q}^-$ interval is scaled by 1/2, and the $c_{t\phi}$ interval is scaled by 1/5.

Table 5: The 2σ confidence intervals on the WCs. The intervals are found by scanning over a single WC while either treating the other 15 profiled, or fixing the other 15 to the SM value of zero.

WC/ Λ^2 [TeV $^{-2}$]	2σ interval (others profiled)	2σ interval (others fixed to SM)
c_{tW}	[-3.08, 2.87]	[-2.15, -0.29] \cup [0.21, 1.96]
c_{tZ}	[-3.32, 3.15]	[-2.14, 2.19]
$c_{t\varphi}$	[-16.98, 44.26]	[-14.12, -1.46] \cup [32.30, 44.48]
$c_{\varphi Q}^-$	[-7.59, 21.65]	[-3.45, 3.33]
c_{tG}	[-1.38, 1.18]	[-1.26, -0.69] \cup [0.08, 0.79]
c_{bW}	[-4.95, 4.95]	[-4.12, 4.09]
$c_{\varphi Q}^3$	[-7.37, 3.48]	[-7.21, 2.25]
$c_{\varphi tb}$	[-12.72, 12.63]	[-9.87, 9.67]
$c_{\varphi t}$	[-18.62, 12.31]	[-20.91, -14.10] \cup [-6.52, 4.24]
$c_{Q\ell}^{3(\ell)}$	[-9.67, 8.97]	[-9.91, 9.50]
$c_{Q\ell}^{-(\ell)}$	[-4.02, 4.99]	[-4.76, 5.83]
$c_{Qe}^{(\ell)}$	[-4.38, 4.59]	[-5.20, 5.36]
$c_{t\ell}^{(\ell)}$	[-4.29, 4.82]	[-5.15, 5.51]
$c_{te}^{(\ell)}$	[-4.24, 4.86]	[-4.97, 5.80]
$c_t^{S(\ell)}$	[-6.52, 6.52]	[-7.70, 7.70]
$c_t^{T(\ell)}$	[-0.84, 0.84]	[-1.01, 1.01]

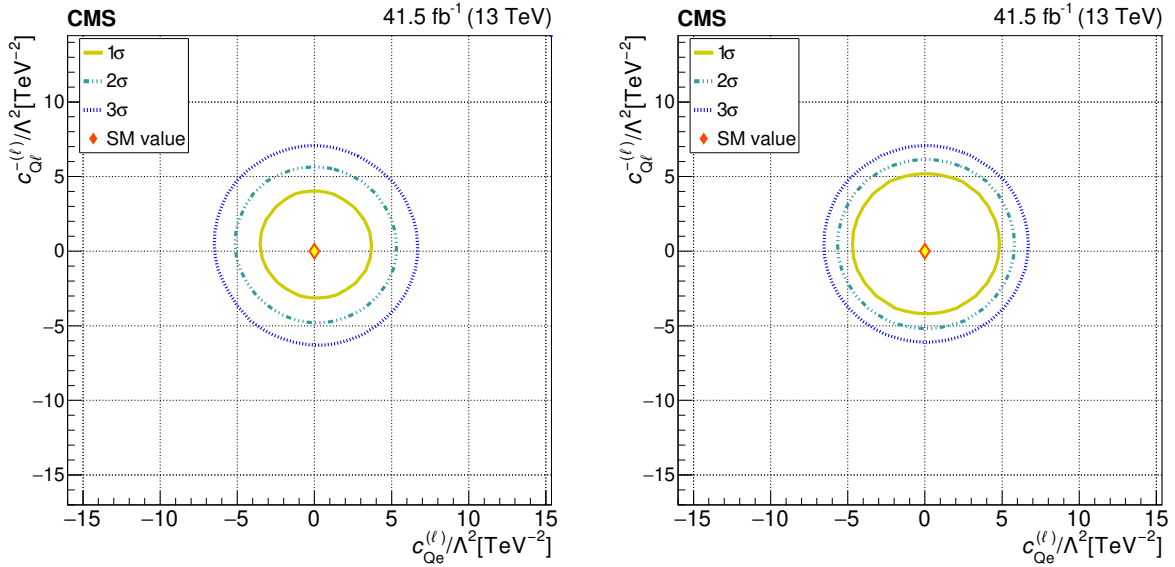


Figure 5: The observed 1σ , 2σ , and 3σ confidence contours of a 2D scan for $c_{Q\ell}^{-(\ell)}$ and $c_{Qe}^{(\ell)}$ with the other WCs profiled (left), and fixed to their SM values (right). Diamond markers are shown for the SM prediction.

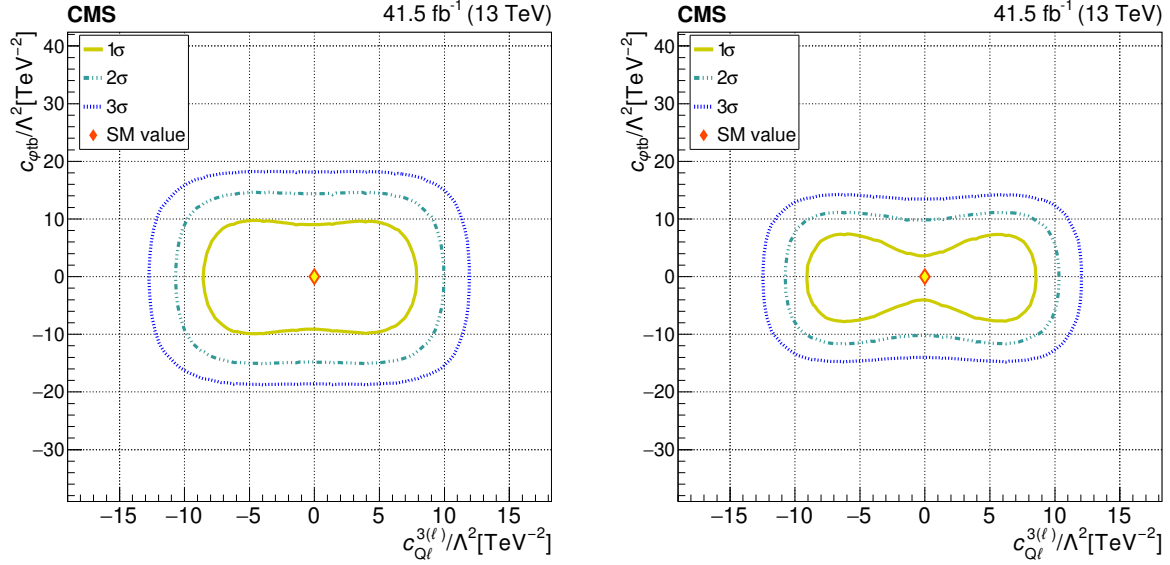


Figure 6: The observed 1σ , 2σ , and 3σ confidence contours of a 2D scan for $c_{\varphi tb}$ and $c_{Q\ell}^{3(\ell)}$ with the other WCs profiled (left), and fixed to their SM values (right). Diamond markers are shown for the SM prediction.

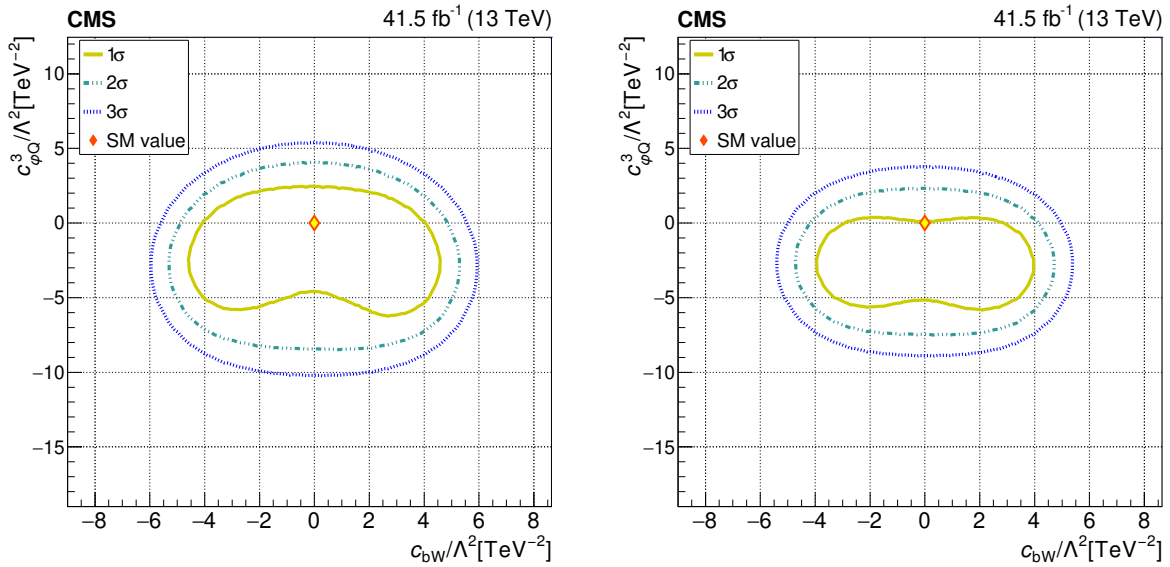


Figure 7: The observed 1σ , 2σ , and 3σ confidence contours of a 2D scan for $c_{\varphi Q}^3$ and c_{bW} with the other WCs profiled (left), and fixed to their SM values (right). Diamond markers are shown for the SM prediction.

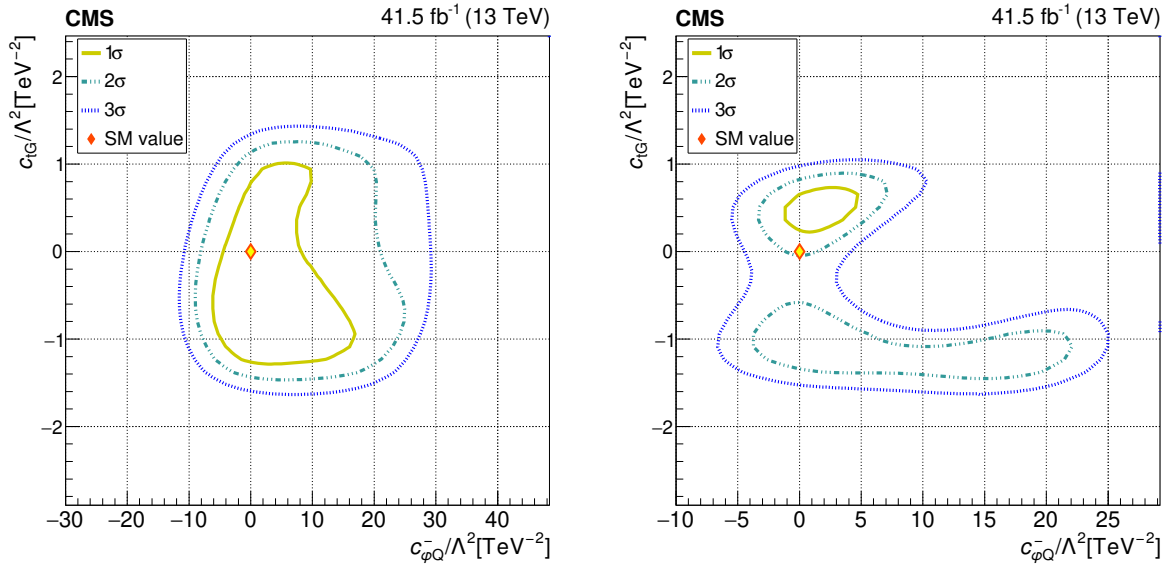


Figure 8: The observed 1σ , 2σ , and 3σ confidence contours of a 2D scan for c_{tG} and $c_{\varphi Q}^-$ with the other WCs profiled (left), and fixed to their SM values (right). Diamond markers are shown for the SM prediction. The range on the right plot is modified to emphasize the 1σ contour.

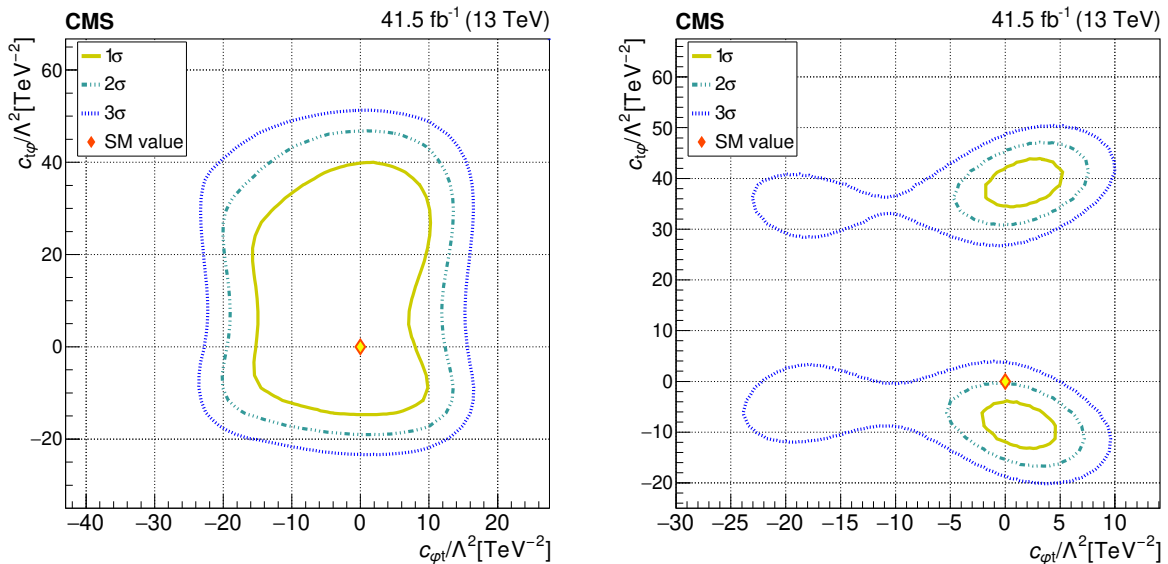


Figure 9: The observed 1σ , 2σ , and 3σ confidence contours of a 2D scan for $c_{t\varphi}$ and $c_{\varphi t}$ with the other WCs profiled (left), and fixed to their SM values (right). Diamond markers are shown for the SM prediction. The range on the right plot is modified to emphasize the 1σ contour.

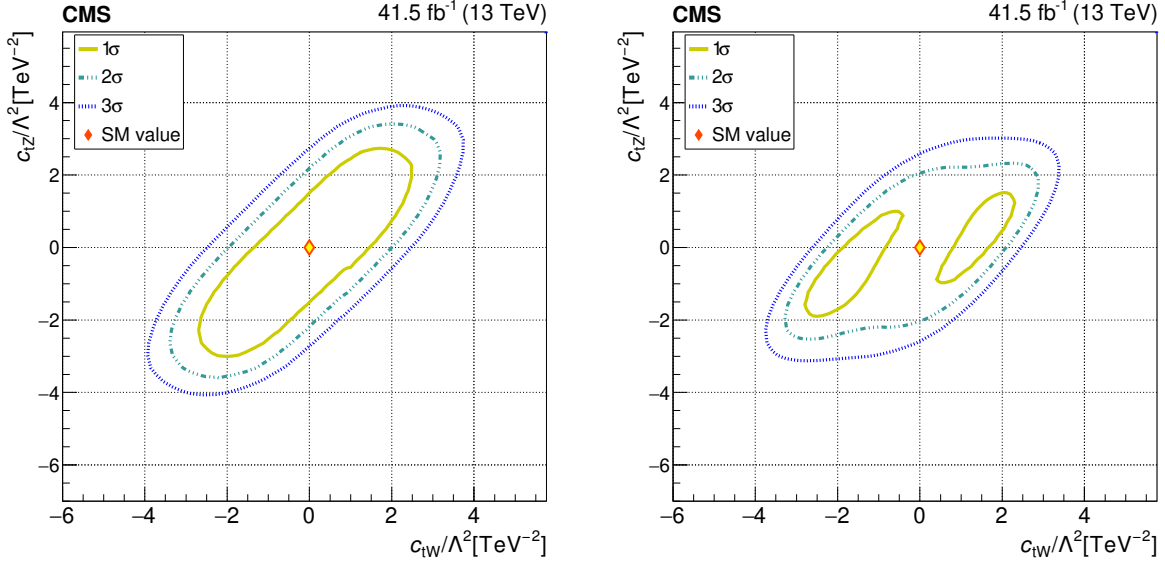


Figure 10: The observed 1σ , 2σ , and 3σ confidence contours of a 2D scan for c_{tZ} and c_{tW} with the other WCs profiled (left), and fixed to their SM values (right). Diamond markers are shown for the SM prediction.

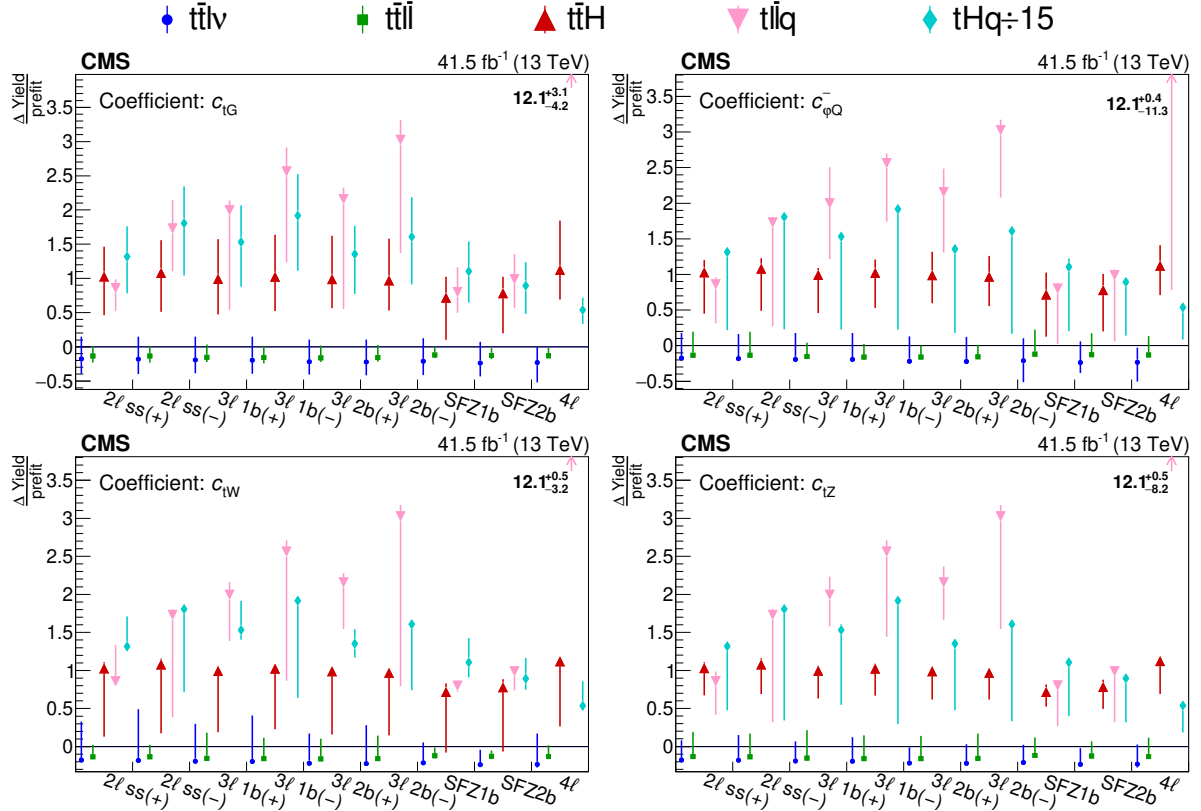


Figure 11: Plots showing the relative change in the expected yield for the signal processes in each event category. The “ $\Delta\text{Yield}/\text{prefit}$ ” is the difference in expected yield before fit (prefit) and after fit (postfit), normalized to the prefit yield of the process in the corresponding category. The vertical bars represent the maximum variation for a given WC within the corresponding 2σ confidence interval. The values in upper right of each plot are to indicate the variation for $t\bar{l}lq$ in the 4ℓ category.

10 Summary

A search for new physics has been performed in the production of at least one top quark in association with additional leptons, jets, and b jets, in the context of an effective field theory. The events were produced in proton-proton collisions corresponding to an integrated luminosity of 41.5 fb^{-1} . The expected yield in each category was parameterized in terms of 16 Wilson coefficients (WCs) associated with effective field theory operators relevant to the dominant processes in the data.

A simultaneous fit was performed of the 16 WCs to the data. For each WC, an interval over which the model predictions agree with the observed yields at the 2 standard deviation level was extracted by either keeping the other WCs fixed to zero or treating the other WCs as unconstrained nuisance parameters. Two-dimensional contours were produced for some of the WCs, to illustrate correlations between various WCs. The results from fitting the WCs in the dimension-six model to the data were consistent with the standard model at the level of 2 standard deviations.

Acknowledgments

We thank Adam Martin and Jeong Han Kim for their theoretical guidance in configuring and debugging the EFT model used to generate the signal samples in this analysis.

We congratulate our colleagues in the CERN accelerator departments for the excellent performance of the LHC and thank the technical and administrative staffs at CERN and at other CMS institutes for their contributions to the success of the CMS effort. In addition, we gratefully acknowledge the computing centers and personnel of the Worldwide LHC Computing Grid for delivering so effectively the computing infrastructure essential to our analyses. Finally, we acknowledge the enduring support for the construction and operation of the LHC and the CMS detector provided by the following funding agencies: BMBWF and FWF (Austria); FNRS and FWO (Belgium); CNPq, CAPES, FAPERJ, FAPERGS, and FAPESP (Brazil); MES (Bulgaria); CERN; CAS, MoST, and NSFC (China); COLCIENCIAS (Colombia); MSES and CSF (Croatia); RIF (Cyprus); SENESCYT (Ecuador); MoER, ERC PUT and ERDF (Estonia); Academy of Finland, MEC, and HIP (Finland); CEA and CNRS/IN2P3 (France); BMBF, DFG, and HGF (Germany); GSRT (Greece); NKFI (Hungary); DAE and DST (India); IPM (Iran); SFI (Ireland); INFN (Italy); MSIP and NRF (Republic of Korea); MES (Latvia); LAS (Lithuania); MOE and UM (Malaysia); BUAP, CINVESTAV, CONACYT, LNS, SEP, and UASLP-FAI (Mexico); MOS (Montenegro); MBIE (New Zealand); PAEC (Pakistan); MSHE and NSC (Poland); FCT (Portugal); JINR (Dubna); MON, RosAtom, RAS, RFBR, and NRC KI (Russia); MESTD (Serbia); SEIDI, CPAN, PCTI, and FEDER (Spain); MOSTR (Sri Lanka); Swiss Funding Agencies (Switzerland); MST (Taipei); ThEPCenter, IPST, STAR, and NSTDA (Thailand); TUBITAK and TAEK (Turkey); NASU (Ukraine); STFC (United Kingdom); DOE and NSF (USA).

Individuals have received support from the Marie-Curie program and the European Research Council and Horizon 2020 Grant, contract Nos. 675440, 724704, 752730, and 765710 (European Union); the Leventis Foundation; the A.P. Sloan Foundation; the Alexander von Humboldt Foundation; the Belgian Federal Science Policy Office; the Fonds pour la Formation à la Recherche dans l'Industrie et dans l'Agriculture (FRIA-Belgium); the Agentschap voor Innovatie door Wetenschap en Technologie (IWT-Belgium); the F.R.S.-FNRS and FWO (Belgium) under the "Excellence of Science – EOS" – be.h project n. 30820817; the Beijing Municipal Science & Technology Commission, No. Z191100007219010; the Ministry of Education, Youth and Sports (MEYS) of the Czech Republic; the Deutsche Forschungsgemeinschaft (DFG) under Germany's

Excellence Strategy – EXC 2121 “Quantum Universe” – 390833306; the Lendület (“Momentum”) Program and the János Bolyai Research Scholarship of the Hungarian Academy of Sciences, the New National Excellence Program ÚNKP, the NKFI research grants 123842, 123959, 124845, 124850, 125105, 128713, 128786, and 129058 (Hungary); the Council of Science and Industrial Research, India; the HOMING PLUS program of the Foundation for Polish Science, cofinanced from European Union, Regional Development Fund, the Mobility Plus program of the Ministry of Science and Higher Education, the National Science Center (Poland), contracts Harmonia 2014/14/M/ST2/00428, Opus 2014/13/B/ST2/02543, 2014/15/B/ST2/03998, and 2015/19/B/ST2/02861, Sonata-bis 2012/07/E/ST2/01406; the National Priorities Research Program by Qatar National Research Fund; the Ministry of Science and Higher Education, project no. 0723-2020-0041 (Russia); the Tomsk Polytechnic University Competitiveness Enhancement Program; the Programa Estatal de Fomento de la Investigación Científica y Técnica de Excelencia María de Maeztu, grant MDM-2015-0509 and the Programa Severo Ochoa del Principado de Asturias; the Thalís and Aristeia programs cofinanced by EU-ESF and the Greek NSRF; the Rachadapisek Sompot Fund for Postdoctoral Fellowship, Chulalongkorn University and the Chulalongkorn Academic into Its 2nd Century Project Advancement Project (Thailand); the Kavli Foundation; the Nvidia Corporation; the SuperMicro Corporation; the Welch Foundation, contract C-1845; and the Weston Havens Foundation (USA).

References

- [1] J. L. Feng, “Dark matter candidates from particle physics and methods of detection”, *Ann. Rev. Astron. Astrophys.* **48** (2010) 495, doi:10.1146/annurev-astro-082708-101659, arXiv:1003.0904.
- [2] T. A. Porter, R. P. Johnson, and P. W. Graham, “Dark matter searches with astroparticle data”, *Ann. Rev. Astron. Astrophys.* **49** (2011) 155, doi:10.1146/annurev-astro-081710-102528, arXiv:1104.2836.
- [3] P. J. E. Peebles and B. Ratra, “The cosmological constant and dark energy”, *Rev. Mod. Phys.* **75** (2003) 559, doi:10.1103/RevModPhys.75.559, arXiv:astro-ph/0207347.
- [4] Particle Data Group, “Review of particle physics”, *PTEP* **2020** (2020) 083C01, doi:10.1093/ptep/ptaa104.
- [5] E. Witten, “Dynamical breaking of supersymmetry”, *Nucl. Phys. B* **188** (1981) 513, doi:10.1016/0550-3213(81)90006-7.
- [6] J. Alimena et al., “Searching for long-lived particles beyond the standard model at the Large Hadron Collider”, *J. Phys. G* **47** (2020) 090501, doi:10.1088/1361-6471/ab4574, arXiv:1903.04497.
- [7] O. Matsedonskyi, G. Panico, and A. Wulzer, “Light top partners for a light composite Higgs”, *JHEP* **01** (2013) 164, doi:10.1007/JHEP01(2013)164, arXiv:1204.6333.
- [8] W. Buchmuller and D. Wyler, “Effective Lagrangian analysis of new interactions and flavor conservation”, *Nucl. Phys. B* **268** (1986) 621, doi:10.1016/0550-3213(86)90262-2.
- [9] B. Grzadkowski, M. Iskrzynski, M. Misiak, and J. Rosiek, “Dimension-six terms in the standard model Lagrangian”, *JHEP* **10** (2010) 085, doi:10.1007/JHEP10(2010)085, arXiv:1008.4884.

- [10] A. Falkowski and R. Rattazzi, “Which EFT”, *JHEP* **10** (2019) 255, doi:10.1007/JHEP10(2019)255, arXiv:1902.05936.
- [11] C. Degrande et al., “Effective field theory: a modern approach to anomalous couplings”, *Annals Phys.* **335** (2013) 21, doi:10.1016/j.aop.2013.04.016, arXiv:1205.4231.
- [12] CDF Collaboration, “Observation of top quark production in $\bar{p}p$ collisions”, *Phys. Rev. Lett.* **74** (1995) 2626, doi:10.1103/PhysRevLett.74.2626, arXiv:hep-ex/9503002.
- [13] D0 Collaboration, “Observation of the top quark”, *Phys. Rev. Lett.* **74** (1995) 2632, doi:10.1103/PhysRevLett.74.2632, arXiv:hep-ex/9503003.
- [14] CMS Collaboration, “Observation of $t\bar{t}H$ production”, *Phys. Rev. Lett.* **120** (2018) 231801, doi:10.1103/PhysRevLett.120.231801, arXiv:1804.02610.
- [15] ATLAS Collaboration, “Observation of Higgs boson production in association with a top quark pair at the LHC with the ATLAS detector”, *Phys. Lett. B* **784** (2018) 173, doi:10.1016/j.physletb.2018.07.035, arXiv:1806.00425.
- [16] CMS Collaboration, “Measurement of the cross section for top quark pair production in association with a W or Z boson in proton-proton collisions at $\sqrt{s} = 13$ TeV”, *JHEP* **08** (2018) 011, doi:10.1007/JHEP08(2018)011, arXiv:1711.02547.
- [17] CMS Collaboration, “Observation of single top quark production in association with a Z boson in proton-proton collisions at $\sqrt{s} = 13$ TeV”, *Phys. Rev. Lett.* **122** (2019) 132003, doi:10.1103/PhysRevLett.122.132003, arXiv:1812.05900.
- [18] ATLAS Collaboration, “Measurement of the $t\bar{t}Z$ and $t\bar{t}W$ cross sections in proton-proton collisions at $\sqrt{s} = 13$ TeV with the ATLAS detector”, *Phys. Rev. D* **99** (2019) 072009, doi:10.1103/PhysRevD.99.072009, arXiv:1901.03584.
- [19] CMS Collaboration, “Measurements of $t\bar{t}$ differential cross sections in proton-proton collisions at $\sqrt{s} = 13$ TeV using events containing two leptons”, *JHEP* **02** (2019) 149, doi:10.1007/JHEP02(2019)149, arXiv:1811.06625.
- [20] CMS Collaboration, “Search for new physics in top quark production in dilepton final states in proton-proton collisions at $\sqrt{s} = 13$ TeV”, *Eur. Phys. J. C* **79** (2019) 886, doi:10.1140/epjc/s10052-019-7387-y, arXiv:1903.11144.
- [21] CMS Collaboration, “Measurement of the top quark polarization and $t\bar{t}$ spin correlations using dilepton final states in proton-proton collisions at $\sqrt{s} = 13$ TeV”, *Phys. Rev. D* **100** (2019) 072002, doi:10.1103/PhysRevD.100.072002, arXiv:1907.03729.
- [22] CMS Collaboration, “Measurement of top quark pair production in association with a Z boson in proton-proton collisions at $\sqrt{s} = 13$ TeV”, *JHEP* **03** (2020) 056, doi:10.1007/JHEP03(2020)056, arXiv:1907.11270.
- [23] ATLAS Collaboration, “Search for flavour-changing neutral currents in processes with one top quark and a photon using 81 fb^{-1} of pp collisions at $\sqrt{s} = 13$ TeV with the ATLAS experiment”, *Phys. Lett. B* **800** (2020) 135082, doi:10.1016/j.physletb.2019.135082, arXiv:1908.08461.

-
- [24] ATLAS Collaboration, “Search for flavour-changing neutral current top-quark decays $t \rightarrow qZ$ in proton-proton collisions at $\sqrt{s} = 13$ TeV with the ATLAS detector”, *JHEP* **07** (2018) 176, doi:10.1007/JHEP07(2018)176, arXiv:1803.09923.
- [25] A. Buckley et al., “Constraining top quark effective theory in the LHC Run II era”, *JHEP* **04** (2016) 015, doi:10.1007/JHEP04(2016)015, arXiv:1512.03360.
- [26] N. P. Hartland et al., “A Monte Carlo global analysis of the standard model effective field theory: the top quark sector”, *JHEP* **04** (2019) 100, doi:10.1007/JHEP04(2019)100, arXiv:1901.05965.
- [27] I. Brivio et al., “O new physics, where art thou? A global search in the top sector”, *JHEP* **02** (2020) 131, doi:10.1007/JHEP02(2020)131, arXiv:1910.03606.
- [28] CMS Collaboration, “The CMS experiment at the CERN LHC”, *JINST* **3** (2008) S08004, doi:10.1088/1748-0221/3/08/S08004.
- [29] CMS Collaboration, “The CMS trigger system”, *JINST* **12** (2017) P01020, doi:10.1088/1748-0221/12/01/P01020, arXiv:1609.02366.
- [30] CMS Collaboration, “CMS luminosity measurement for the 2017 data-taking period at $\sqrt{s} = 13$ TeV”, CMS Physics Analysis Summary CMS-PAS-LUM-17-004, 2018.
- [31] J. Alwall et al., “The automated computation of tree-level and next-to-leading order differential cross sections, and their matching to parton shower simulations”, *JHEP* **07** (2014) 079, doi:10.1007/JHEP07(2014)079, arXiv:1405.0301.
- [32] R. Frederix and S. Frixione, “Merging meets matching in MC@NLO”, *JHEP* **12** (2012) 061, doi:10.1007/JHEP12(2012)061, arXiv:1209.6215.
- [33] J. Alwall et al., “Comparative study of various algorithms for the merging of parton showers and matrix elements in hadronic collisions”, *Eur. Phys. J. C* **53** (2008) 473, doi:10.1140/epjc/s10052-007-0490-5, arXiv:0706.2569.
- [34] P. Nason, “A new method for combining NLO QCD with shower Monte Carlo algorithms”, *JHEP* **11** (2004) 040, doi:10.1088/1126-6708/2004/11/040, arXiv:hep-ph/0409146.
- [35] S. Frixione, P. Nason, and C. Oleari, “Matching NLO QCD computations with parton shower simulations: the POWHEG method”, *JHEP* **11** (2007) 070, doi:10.1088/1126-6708/2007/11/070, arXiv:0709.2092.
- [36] S. Alioli, P. Nason, C. Oleari, and E. Re, “A general framework for implementing NLO calculations in shower Monte Carlo programs: the POWHEG BOX”, *JHEP* **06** (2010) 043, doi:10.1007/JHEP06(2010)043, arXiv:1002.2581.
- [37] R. Frederix, E. Re, and P. Torrielli, “Single-top t-channel hadroproduction in the four-flavour scheme with POWHEG and aMC@NLO”, *JHEP* **09** (2012) 130, doi:10.1007/JHEP09(2012)130, arXiv:1207.5391.
- [38] E. Re, “Single-top Wt-channel production matched with parton showers using the POWHEG method”, *Eur. Phys. J. C* **71** (2011) 1547, doi:10.1140/epjc/s10052-011-1547-z, arXiv:1009.2450.

- [39] T. Melia, P. Nason, R. Rontsch, and G. Zanderighi, “ W^+W^- , WZ and ZZ production in the POWHEG BOX”, *JHEP* **11** (2011) 078, doi:10.1007/JHEP11(2011)078, arXiv:1107.5051.
- [40] S. Frixione, P. Nason, and G. Ridolfi, “A positive-weight next-to-leading-order Monte Carlo for heavy flavour hadroproduction”, *JHEP* **09** (2007) 126, doi:10.1088/1126-6708/2007/09/126, arXiv:0707.3088.
- [41] T. Sjöstrand et al., “An introduction to PYTHIA 8.2”, *Comput. Phys. Commun.* **191** (2015) 159, doi:10.1016/j.cpc.2015.01.024, arXiv:1410.3012.
- [42] P. Skands, S. Carrazza, and J. Rojo, “Tuning PYTHIA 8.1: the Monash 2013 tune”, *Eur. Phys. J. C* **74** (2014) 3024, doi:10.1140/epjc/s10052-014-3024-y, arXiv:1404.5630.
- [43] CMS Collaboration, “Extraction and validation of a new set of CMS PYTHIA8 tunes from underlying-event measurements”, *Eur. Phys. J. C* **80** (2020) 4, doi:10.1140/epjc/s10052-019-7499-4, arXiv:1903.12179.
- [44] NNPDF Collaboration, “Parton distributions for the LHC Run II”, *JHEP* **04** (2015) 040, doi:10.1007/JHEP04(2015)040, arXiv:1410.8849.
- [45] GEANT4 Collaboration, “GEANT4—a simulation toolkit”, *Nucl. Instrum. Meth. A* **506** (2003) 250, doi:10.1016/S0168-9002(03)01368-8.
- [46] D. Barducci et al., “Interpreting top-quark LHC measurements in the standard-model effective field theory”, 2018. arXiv:1802.07237.
- [47] LHC Higgs Cross Section Working Group, “Handbook of LHC Higgs cross sections: 4. deciphering the nature of the Higgs sector”, CERN (2016) doi:10.23731/CYRM-2017-002, arXiv:1610.07922.
- [48] CMS Collaboration, “Particle-flow reconstruction and global event description with the cms detector”, *JINST* **12** (2017) P10003, doi:10.1088/1748-0221/12/10/P10003, arXiv:1706.04965.
- [49] CMS Collaboration, “Performance of missing transverse momentum reconstruction in proton-proton collisions at $\sqrt{s} = 13$ TeV using the CMS detector”, *JINST* **14** (2019) P07004, doi:10.1088/1748-0221/14/07/P07004, arXiv:1903.06078.
- [50] M. Cacciari, G. P. Salam, and G. Soyez, “The anti- k_t jet clustering algorithm”, *JHEP* **04** (2008) 063, doi:10.1088/1126-6708/2008/04/063, arXiv:0802.1189.
- [51] M. Cacciari, G. P. Salam, and G. Soyez, “FASTJET user manual”, *Eur. Phys. J. C* **72** (2012) 1896, doi:10.1140/epjc/s10052-012-1896-2, arXiv:1111.6097.
- [52] CMS Collaboration, “Technical Proposal for the Phase-II Upgrade of the CMS Detector”, Technical Report CERN-LHCC-2015-010. LHCC-P-008. CMS-TDR-15-02, CERN, 2015.
- [53] CMS Collaboration, “Performance of electron reconstruction and selection with the CMS detector in proton-proton collisions at $\sqrt{s} = 8$ TeV”, *JINST* **10** (2015) P06005, doi:10.1088/1748-0221/10/06/P06005, arXiv:1502.02701.
- [54] CMS Collaboration, “Performance of the CMS muon detector and muon reconstruction with proton-proton collisions at $\sqrt{s} = 13$ TeV”, *JINST* **13** (2018) P06015, doi:10.1088/1748-0221/13/06/P06015, arXiv:1804.04528.

- [55] CMS Collaboration, "Performance of CMS muon reconstruction in pp collision events at $\sqrt{s} = 7$ TeV", *JINST* **7** (2012) P10002, doi:10.1088/1748-0221/7/10/P10002, arXiv:1206.4071.
- [56] CMS Collaboration, "Evidence for associated production of a Higgs boson with a top quark pair in final states with electrons, muons, and hadronically decaying τ leptons at $\sqrt{s} = 13$ TeV", *JHEP* **08** (2018) 066, doi:10.1007/JHEP08(2018)066, arXiv:1803.05485.
- [57] CMS Collaboration, "Jet energy scale and resolution in the CMS experiment in pp collisions at 8 TeV", *JINST* **12** (2017) P02014, doi:10.1088/1748-0221/12/02/P02014, arXiv:1607.03663.
- [58] CMS Collaboration, "Identification of b quark jets with the CMS experiment", *JINST* **8** (2013) P04013, doi:10.1088/1748-0221/8/04/P04013, arXiv:1211.4462.
- [59] CMS Collaboration, "Identification of heavy-flavour jets with the CMS detector in pp collisions at 13 TeV", *JINST* **13** (2018) P05011, doi:10.1088/1748-0221/13/05/P05011, arXiv:1712.07158.
- [60] J. Butterworth et al., "PDF4LHC recommendations for LHC Run II", *J. Phys. G* **43** (2016) 023001, doi:10.1088/0954-3899/43/2/023001, arXiv:1510.03865.
- [61] CMS Collaboration, "Measurements of inclusive W and Z cross sections in pp collisions at $\sqrt{s} = 7$ TeV", *JHEP* **01** (2011) 080, doi:10.1007/JHEP01(2011)080, arXiv:1012.2466.
- [62] ATLAS Collaboration, "Measurement of the inelastic proton-proton cross section at $\sqrt{s} = 13$ TeV with the ATLAS detector at the LHC", *Phys. Rev. Lett.* **117** (2016) 182002, doi:10.1103/PhysRevLett.117.182002, arXiv:1606.02625.

A The CMS Collaboration

Yerevan Physics Institute, Yerevan, Armenia

A.M. Sirunyan[†], A. Tumasyan

Institut für Hochenergiephysik, Wien, Austria

W. Adam, T. Bergauer, M. Dragicevic, A. Escalante Del Valle, R. Frühwirth¹, M. Jeitler¹, N. Krammer, L. Lechner, D. Liko, I. Mikulec, F.M. Pitters, N. Rad, J. Schieck¹, R. Schöffbeck, M. Spanring, S. Templ, W. Waltenberger, C.-E. Wulz¹, M. Zarucki

Institute for Nuclear Problems, Minsk, Belarus

V. Chekhovskiy, A. Litomin, V. Makarenko, J. Suarez Gonzalez

Universiteit Antwerpen, Antwerpen, Belgium

M.R. Darwish², E.A. De Wolf, X. Janssen, T. Kello³, A. Lelek, M. Pieters, H. Rejeb Sfar, H. Van Haeve, P. Van Mechelen, S. Van Putte, N. Van Remortel

Vrije Universiteit Brussel, Brussel, Belgium

F. Blekman, E.S. Bols, S.S. Chhibra, J. D'Hondt, J. De Clercq, D. Lontkovskiy, S. Lowette, I. Marchesini, S. Moortgat, A. Morton, D. Müller, Q. Python, S. Tavernier, W. Van Doninck, P. Van Mulders

Université Libre de Bruxelles, Bruxelles, Belgium

D. Beghin, B. Bilin, B. Clerbaux, G. De Lentdecker, B. Dorney, L. Favart, A. Grebenyuk, A.K. Kalsi, I. Makarenko, L. Moureaux, L. Pétré, A. Popov, N. Postiau, E. Starling, L. Thomas, C. Vander Velde, P. Vanlaer, D. Vannerom, L. Wezenbeek

Ghent University, Ghent, Belgium

T. Cornelis, D. Dobur, M. Gruchala, I. Khvastunov⁴, G. Mestdach, M. Niedziela, C. Roskas, K. Skovpen, M. Tytgat, W. Verbeke, B. Vermassen, M. Vit

Université Catholique de Louvain, Louvain-la-Neuve, Belgium

G. Bruno, F. Bury, C. Caputo, P. David, C. Delaere, M. Delcourt, I.S. Donertas, A. Giammanco, V. Lemaître, K. Mondal, J. Prisciandaro, A. Taliencio, M. Teklishyn, P. Vischia, S. Wertz, S. Wuyckens

Centro Brasileiro de Pesquisas Físicas, Rio de Janeiro, Brazil

G.A. Alves, C. Hensel, A. Moraes

Universidade do Estado do Rio de Janeiro, Rio de Janeiro, Brazil

W.L. Aldá Júnior, E. Belchior Batista Das Chagas, H. BRANDAO MALBOUISSON, W. Carvalho, J. Chinellato⁵, E. Coelho, E.M. Da Costa, G.G. Da Silveira⁶, D. De Jesus Damiao, S. Fonseca De Souza, J. Martins⁷, D. Matos Figueiredo, M. Medina Jaime⁸, C. Mora Herrera, L. Mundim, H. Nogima, P. Rebello Teles, L.J. Sanchez Rosas, A. Santoro, S.M. Silva Do Amaral, A. Sznajder, M. Thiel, F. Torres Da Silva De Araujo, A. Vilela Pereira

Universidade Estadual Paulista ^a, Universidade Federal do ABC ^b, São Paulo, Brazil

C.A. Bernardes^{a,a}, L. Calligaris^a, T.R. Fernandez Perez Tomei^a, E.M. Gregores^{a,b}, D.S. Lemos^a, P.G. Mercadante^{a,b}, S.F. Novaes^a, Sandra S. Padula^a

Institute for Nuclear Research and Nuclear Energy, Bulgarian Academy of Sciences, Sofia, Bulgaria

A. Aleksandrov, G. Antchev, I. Atanasov, R. Hadjiiska, P. Iaydjiev, M. Misheva, M. Rodozov, M. Shopova, G. Sultanov

University of Sofia, Sofia, Bulgaria

A. Dimitrov, T. Ivanov, L. Litov, B. Pavlov, P. Petkov, A. Petrov

Beihang University, Beijing, China

T. Cheng, W. Fang³, Q. Guo, H. Wang, L. Yuan

Department of Physics, Tsinghua University, Beijing, China

M. Ahmad, G. Bauer, Z. Hu, Y. Wang, K. Yi^{9,10}

Institute of High Energy Physics, Beijing, China

E. Chapon, G.M. Chen¹¹, H.S. Chen¹¹, M. Chen, T. Javaid¹¹, A. Kapoor, D. Leggat, H. Liao, Z.-A. LIU¹¹, R. Sharma, A. Spiezia, J. Tao, J. Thomas-wilsker, J. Wang, H. Zhang, S. Zhang¹¹, J. Zhao

State Key Laboratory of Nuclear Physics and Technology, Peking University, Beijing, China

A. Agapitos, Y. Ban, C. Chen, Q. Huang, A. Levin, Q. Li, M. Lu, X. Lyu, Y. Mao, S.J. Qian, D. Wang, Q. Wang, J. Xiao

Sun Yat-Sen University, Guangzhou, China

Z. You

Institute of Modern Physics and Key Laboratory of Nuclear Physics and Ion-beam Application (MOE) - Fudan University, Shanghai, China

X. Gao³

Zhejiang University, Hangzhou, China

M. Xiao

Universidad de Los Andes, Bogota, Colombia

C. Avila, A. Cabrera, C. Florez, J. Fraga, A. Sarkar, M.A. Segura Delgado

Universidad de Antioquia, Medellin, Colombia

J. Jaramillo, J. Mejia Guisao, F. Ramirez, J.D. Ruiz Alvarez, C.A. Salazar González, N. Vanegas Arbelaez

University of Split, Faculty of Electrical Engineering, Mechanical Engineering and Naval Architecture, Split, Croatia

D. Giljanovic, N. Godinovic, D. Lelas, I. Puljak

University of Split, Faculty of Science, Split, Croatia

Z. Antunovic, M. Kovac, T. Sculac

Institute Rudjer Boskovic, Zagreb, Croatia

V. Brigljevic, D. Ferencek, D. Majumder, M. Roguljic, A. Starodumov¹², T. Susa

University of Cyprus, Nicosia, Cyprus

M.W. Ather, A. Attikis, E. Erodou, A. Ioannou, G. Kole, M. Kolosova, S. Konstantinou, J. Mousa, C. Nicolaou, F. Ptochos, P.A. Razis, H. Rykaczewski, H. Saka, D. Tsiakkouri

Charles University, Prague, Czech Republic

M. Finger¹³, M. Finger Jr.¹³, A. Kveton, J. Tomsa

Escuela Politecnica Nacional, Quito, Ecuador

E. Ayala

Universidad San Francisco de Quito, Quito, Ecuador

E. Carrera Jarrin

Academy of Scientific Research and Technology of the Arab Republic of Egypt, Egyptian Network of High Energy Physics, Cairo, Egypt

A.A. Abdelalim^{14,15}, S. Abu Zeid¹⁶, S. Elgammal¹⁷

Center for High Energy Physics (CHEP-FU), Fayoum University, El-Fayoum, Egypt

A. Lotfy, M.A. Mahmoud

National Institute of Chemical Physics and Biophysics, Tallinn, Estonia

S. Bhowmik, A. Carvalho Antunes De Oliveira, R.K. Dewanjee, K. Ehataht, M. Kadastik, J. Pata, M. Raidal, C. Veelken

Department of Physics, University of Helsinki, Helsinki, Finland

P. Eerola, L. Forthomme, H. Kirschenmann, K. Osterberg, M. Voutilainen

Helsinki Institute of Physics, Helsinki, Finland

E. Brücken, F. Garcia, J. Havukainen, V. Karimäki, M.S. Kim, R. Kinnunen, T. Lampén, K. Lassila-Perini, S. Lehti, T. Lindén, H. Siikonen, E. Tuominen, J. Tuominiemi

Lappeenranta University of Technology, Lappeenranta, Finland

P. Luukka, T. Tuuva

IRFU, CEA, Université Paris-Saclay, Gif-sur-Yvette, France

C. Amendola, M. Besancon, F. Couderc, M. Dejardin, D. Denegri, J.L. Faure, F. Ferri, S. Ganjour, A. Givernaud, P. Gras, G. Hamel de Monchenault, P. Jarry, B. Lenzi, E. Locci, J. Malcles, J. Rander, A. Rosowsky, M.Ö. Sahin, A. Savoy-Navarro¹⁸, M. Titov, G.B. Yu

Laboratoire Leprince-Ringuet, CNRS/IN2P3, Ecole Polytechnique, Institut Polytechnique de Paris, Palaiseau, France

S. Ahuja, F. Beaudette, M. Bonanomi, A. Buchot Perraguin, P. Busson, C. Charlot, O. Davignon, B. Diab, G. Falmagne, R. Granier de Cassagnac, A. Hakimi, I. Kucher, A. Lobanov, C. Martin Perez, M. Nguyen, C. Ochando, P. Paganini, J. Rembser, R. Salerno, J.B. Sauvan, Y. Sirois, A. Zabi, A. Zghiche

Université de Strasbourg, CNRS, IPHC UMR 7178, Strasbourg, France

J.-L. Agram¹⁹, J. Andrea, D. Bloch, G. Bourgatte, J.-M. Brom, E.C. Chabert, C. Collard, J.-C. Fontaine¹⁹, D. Gelé, U. Goerlach, C. Grimault, A.-C. Le Bihan, P. Van Hove

Université de Lyon, Université Claude Bernard Lyon 1, CNRS-IN2P3, Institut de Physique Nucléaire de Lyon, Villeurbanne, France

E. Asilar, S. Beauceron, C. Bernet, G. Boudoul, C. Camen, A. Carle, N. Chanon, D. Contardo, P. Depasse, H. El Mamouni, J. Fay, S. Gascon, M. Gouzevitch, B. Ille, Sa. Jain, I.B. Laktineh, H. Lattaud, A. Lesauvage, M. Lethuillier, L. Mirabito, K. Shchablo, L. Torterotot, G. Touquet, M. Vander Donckt, S. Viret

Georgian Technical University, Tbilisi, Georgia

T. Toriashvili²⁰, Z. Tsamalaidze¹³

RWTH Aachen University, I. Physikalisches Institut, Aachen, Germany

L. Feld, K. Klein, M. Lipinski, D. Meuser, A. Pauls, M.P. Rauch, J. Schulz, M. Teroerde

RWTH Aachen University, III. Physikalisches Institut A, Aachen, Germany

D. Eliseev, M. Erdmann, P. Fackeldey, B. Fischer, S. Ghosh, T. Hebbeker, K. Hoepfner, H. Keller, L. Mastrolorenzo, M. Merschmeyer, A. Meyer, G. Mocellin, S. Mondal, S. Mukherjee, D. Noll, A. Novak, T. Pook, A. Pozdnyakov, Y. Rath, H. Reithler, J. Roemer, A. Schmidt, S.C. Schuler, A. Sharma, S. Wiedenbeck, S. Zaleski

RWTH Aachen University, III. Physikalisches Institut B, Aachen, Germany

C. Dziwok, G. Flügge, W. Haj Ahmad²¹, O. Hlushchenko, T. Kress, A. Nowack, C. Pistone, O. Pooth, D. Roy, H. Sert, A. Stahl²², T. Ziemons

Deutsches Elektronen-Synchrotron, Hamburg, Germany

H. Aarup Petersen, M. Aldaya Martin, P. Asmuss, I. Babounikau, S. Baxter, O. Behnke, A. Bermúdez Martínez, A.A. Bin Anuar, K. Borras²³, V. Botta, D. Brunner, A. Campbell, A. Cardini, P. Connor, S. Consuegra Rodríguez, V. Danilov, A. De Wit, M.M. Defranchis, L. Didukh, D. Domínguez Damiani, G. Eckerlin, D. Eckstein, L.I. Estevez Banos, E. Gallo²⁴, A. Geiser, A. Giraldi, A. Grohsjean, M. Guthoff, A. Harb, A. Jafari²⁵, N.Z. Jomhari, H. Jung, A. Kasem²³, M. Kasemann, H. Kaveh, C. Kleinwort, J. Knolle, D. Krücker, W. Lange, T. Lenz, J. Lidrych, K. Lipka, W. Lohmann²⁶, T. Madlener, R. Mankel, I.-A. Melzer-Pellmann, J. Metwally, A.B. Meyer, M. Meyer, J. Mnich, A. Mussgiller, V. Myronenko, Y. Otari, D. Pérez Adán, S.K. Pflitsch, D. Pitzl, A. Raspereza, A. Saggio, A. Saibel, M. Savitskyi, V. Scheurer, C. Schwanenberger, A. Singh, R.E. Sosa Ricardo, N. Tonon, O. Turkot, A. Vagnerini, M. Van De Klundert, R. Walsh, D. Walter, Y. Wen, K. Wichmann, C. Wissing, S. Wuchterl, O. Zenaiev, R. Zlebcik

University of Hamburg, Hamburg, Germany

R. Aggleton, S. Bein, L. Benato, A. Benecke, K. De Leo, T. Dreyer, A. Ebrahimi, M. Eich, F. Feindt, A. Fröhlich, C. Garbers, E. Garutti, P. Gunnellini, J. Haller, A. Hinzmann, A. Karavdina, G. Kasieczka, R. Klanner, R. Kogler, V. Kutzner, J. Lange, T. Lange, A. Malara, C.E.N. Niemeyer, A. Nigamova, K.J. Pena Rodriguez, O. Rieger, P. Schleper, S. Schumann, J. Schwandt, D. Schwarz, J. Sonneveld, H. Stadie, G. Steinbrück, A. Tews, B. Vormwald, I. Zoi

Karlsruher Institut fuer Technologie, Karlsruhe, Germany

J. Bechtel, T. Berger, E. Butz, R. Caspart, T. Chwalek, W. De Boer, A. Dierlamm, A. Droll, K. El Morabit, N. Faltermann, K. Flöh, M. Giffels, A. Gottmann, F. Hartmann²², C. Heidecker, U. Husemann, I. Katkov²⁷, P. Keicher, R. Koppenhöfer, S. Maier, M. Metzler, S. Mitra, Th. Müller, M. Musich, G. Quast, K. Rabbertz, J. Rauser, D. Savoie, D. Schäfer, M. Schnepf, M. Schröder, D. Seith, I. Shvetsov, H.J. Simonis, R. Ulrich, M. Wassmer, M. Weber, R. Wolf, S. Wozniewski

Institute of Nuclear and Particle Physics (INPP), NCSR Demokritos, Aghia Paraskevi, Greece

G. Anagnostou, P. Asenov, G. Daskalakis, T. Geralis, A. Kyriakis, D. Loukas, G. Paspalaki, A. Stakia

National and Kapodistrian University of Athens, Athens, Greece

M. Diamantopoulou, D. Karasavvas, G. Karathanasis, P. Kontaxakis, C.K. Koraka, A. Manousakis-katsikakis, A. Panagiotou, I. Papavergou, N. Saoulidou, K. Theofilatos, E. Tziaferi, K. Vellidis, E. Vourliotis

National Technical University of Athens, Athens, Greece

G. Bakas, K. Kousouris, I. Papakrivopoulos, G. Tsipolitis, A. Zacharopoulou

University of Ioánnina, Ioánnina, Greece

I. Evangelou, C. Foudas, P. Giannios, P. Katsoulis, P. Kokkas, K. Manitaras, N. Manthos, I. Papadopoulos, J. Strologas

MTA-ELTE Lendület CMS Particle and Nuclear Physics Group, Eötvös Loránd University,

Budapest, Hungary

M. Bartók²⁸, M. Csanad, M.M.A. Gadallah²⁹, S. Lökös³⁰, P. Major, K. Mandal, A. Mehta, G. Pasztor, O. Surányi, G.I. Veres

Wigner Research Centre for Physics, Budapest, Hungary

G. Bencze, C. Hajdu, D. Horvath³¹, F. Sikler, V. Veszpremi, G. Vesztergombi[†]

Institute of Nuclear Research ATOMKI, Debrecen, Hungary

S. Czellar, J. Karancsi²⁸, J. Molnar, Z. Szillasi, D. Teyssier

Institute of Physics, University of Debrecen, Debrecen, Hungary

P. Raics, Z.L. Trocsanyi, B. Ujvari

Eszterhazy Karoly University, Karoly Robert Campus, Gyongyos, Hungary

T. Csorgo³³, F. Nemes³³, T. Novak

Indian Institute of Science (IISc), Bangalore, India

S. Choudhury, J.R. Komaragiri, D. Kumar, L. Panwar, P.C. Tiwari

National Institute of Science Education and Research, HBNI, Bhubaneswar, India

S. Bahinipati³⁴, D. Dash, C. Kar, P. Mal, T. Mishra, V.K. Muraleedharan Nair Bindhu, A. Nayak³⁵, N. Sur, S.K. Swain

Panjab University, Chandigarh, India

S. Bansal, S.B. Beri, V. Bhatnagar, G. Chaudhary, S. Chauhan, N. Dhingra³⁶, R. Gupta, A. Kaur, S. Kaur, P. Kumari, M. Meena, K. Sandeep, S. Sharma, J.B. Singh, A.K. Viridi

University of Delhi, Delhi, India

A. Ahmed, A. Bhardwaj, B.C. Choudhary, R.B. Garg, M. Gola, S. Keshri, A. Kumar, M. Naimuddin, P. Priyanka, K. Ranjan, A. Shah

Saha Institute of Nuclear Physics, HBNI, Kolkata, India

M. Bharti³⁷, R. Bhattacharya, S. Bhattacharya, D. Bhowmik, S. Dutta, S. Ghosh, B. Gomber³⁸, M. Maity³⁹, S. Nandan, P. Palit, P.K. Rout, G. Saha, B. Sahu, S. Sarkar, M. Sharan, B. Singh³⁷, S. Thakur³⁷

Indian Institute of Technology Madras, Madras, India

P.K. Behera, S.C. Behera, P. Kalbhor, A. Muhammad, R. Pradhan, P.R. Pujahari, A. Sharma, A.K. Sikdar

Bhabha Atomic Research Centre, Mumbai, India

D. Dutta, V. Kumar, K. Naskar⁴⁰, P.K. Netrakanti, L.M. Pant, P. Shukla

Tata Institute of Fundamental Research-A, Mumbai, India

T. Aziz, M.A. Bhat, S. Dugad, R. Kumar Verma, G.B. Mohanty, U. Sarkar

Tata Institute of Fundamental Research-B, Mumbai, India

S. Banerjee, S. Bhattacharya, S. Chatterjee, R. Chudasama, M. Guchait, S. Karmakar, S. Kumar, G. Majumder, K. Mazumdar, S. Mukherjee, D. Roy

Indian Institute of Science Education and Research (IISER), Pune, India

S. Dube, B. Kansal, S. Pandey, A. Rane, A. Rastogi, S. Sharma

Department of Physics, Isfahan University of Technology, Isfahan, Iran

H. Bakhshiansohi⁴¹, M. Zeinali⁴²

Institute for Research in Fundamental Sciences (IPM), Tehran, IranS. Chenarani⁴³, S.M. Etesami, M. Khakzad, M. Mohammadi Najafabadi**University College Dublin, Dublin, Ireland**

M. Felcini, M. Grunewald

INFN Sezione di Bari ^a, Università di Bari ^b, Politecnico di Bari ^c, Bari, ItalyM. Abbrescia^{a,b}, R. Aly^{a,b,44}, C. Aruta^{a,b}, A. Colaleo^a, D. Creanza^{a,c}, N. De Filippis^{a,c}, M. De Palma^{a,b}, A. Di Florio^{a,b}, A. Di Pilato^{a,b}, W. Elmetenawee^{a,b}, L. Fiore^a, A. Gelmi^{a,b}, M. Gul^a, G. Iaselli^{a,c}, M. Ince^{a,b}, S. Lezki^{a,b}, G. Maggi^{a,c}, M. Maggi^a, I. Margjeka^{a,b}, V. Mastrapasqua^{a,b}, J.A. Merlin^a, S. My^{a,b}, S. Nuzzo^{a,b}, A. Pompili^{a,b}, G. Pugliese^{a,c}, A. Ranieri^a, G. Selvaggi^{a,b}, L. Silvestris^a, F.M. Simone^{a,b}, R. Venditti^a, P. Verwilligen^a**INFN Sezione di Bologna ^a, Università di Bologna ^b, Bologna, Italy**G. Abbiendi^a, C. Battilana^{a,b}, D. Bonacorsi^{a,b}, L. Borgonovi^a, S. Braibant-Giacomelli^{a,b}, R. Campanini^{a,b}, P. Capiluppi^{a,b}, A. Castro^{a,b}, F.R. Cavallo^a, C. Ciocca^a, M. Cuffiani^{a,b}, G.M. Dallavalle^a, T. Diotallevi^{a,b}, F. Fabbri^a, A. Fanfani^{a,b}, E. Fontanesi^{a,b}, P. Giacomelli^a, L. Giommi^{a,b}, C. Grandi^a, L. Guiducci^{a,b}, F. Iemmi^{a,b}, S. Lo Meo^{a,45}, S. Marcellini^a, G. Masetti^a, F.L. Navarria^{a,b}, A. Perrotta^a, F. Primavera^{a,b}, A.M. Rossi^{a,b}, T. Rovelli^{a,b}, G.P. Siroli^{a,b}, N. Tosi^a**INFN Sezione di Catania ^a, Università di Catania ^b, Catania, Italy**S. Albergo^{a,b,46}, S. Costa^{a,b}, A. Di Mattia^a, R. Potenza^{a,b}, A. Tricomi^{a,b,46}, C. Tuve^{a,b}**INFN Sezione di Firenze ^a, Università di Firenze ^b, Firenze, Italy**G. Barbagli^a, A. Cassese^a, R. Ceccarelli^{a,b}, V. Ciulli^{a,b}, C. Civinini^a, R. D'Alessandro^{a,b}, F. Fiori^a, E. Focardi^{a,b}, G. Latino^{a,b}, P. Lenzi^{a,b}, M. Lizzo^{a,b}, M. Meschini^a, S. Paoletti^a, R. Seidita^{a,b}, G. Sguazzoni^a, L. Viliani^a**INFN Laboratori Nazionali di Frascati, Frascati, Italy**

L. Benussi, S. Bianco, D. Piccolo

INFN Sezione di Genova ^a, Università di Genova ^b, Genova, ItalyM. Bozzo^{a,b}, F. Ferro^a, R. Mulargia^{a,b}, E. Robutti^a, S. Tosi^{a,b}**INFN Sezione di Milano-Bicocca ^a, Università di Milano-Bicocca ^b, Milano, Italy**A. Benaglia^a, A. Beschi^{a,b}, F. Brivio^{a,b}, F. Cetorelli^{a,b}, V. Ciriolo^{a,b,22}, F. De Guio^{a,b}, M.E. Dinardo^{a,b}, P. Dini^a, S. Gennai^a, A. Ghezzi^{a,b}, P. Govoni^{a,b}, L. Guzzi^{a,b}, M. Malberti^a, S. Malvezzi^a, A. Massironi^a, D. Menasce^a, F. Monti^{a,b}, L. Moroni^a, M. Paganoni^{a,b}, D. Pedrini^a, S. Ragazzi^{a,b}, T. Tabarelli de Fatis^{a,b}, D. Valsecchi^{a,b,22}, D. Zuolo^{a,b}**INFN Sezione di Napoli ^a, Università di Napoli 'Federico II' ^b, Napoli, Italy, Università della Basilicata ^c, Potenza, Italy, Università G. Marconi ^d, Roma, Italy**S. Buontempo^a, N. Cavallo^{a,c}, A. De Iorio^{a,b}, F. Fabozzi^{a,c}, F. Fienga^a, A.O.M. Iorio^{a,b}, L. Lista^{a,b}, S. Meola^{a,d,22}, P. Paolucci^{a,22}, B. Rossi^a, C. Sciacca^{a,b}**INFN Sezione di Padova ^a, Università di Padova ^b, Padova, Italy, Università di Trento ^c, Trento, Italy**P. Azzi^a, N. Bacchetta^a, D. Bisello^{a,b}, P. Bortignon^a, A. Bragagnolo^{a,b}, R. Carlin^{a,b}, P. Checchia^a, P. De Castro Manzano^a, T. Dorigo^a, F. Gasparini^{a,b}, U. Gasparini^{a,b}, S.Y. Hoh^{a,b}, L. Layer^{a,47}, M. Margoni^{a,b}, A.T. Meneguzzo^{a,b}, M. Presilla^{a,b}, P. Ronchese^{a,b}, R. Rossin^{a,b}, F. Simonetto^{a,b}, G. Strong^a, M. Tosi^{a,b}, H. YARAR^{a,b}, M. Zanetti^{a,b}, P. Zotto^{a,b}, A. Zucchetta^{a,b}, G. Zumerle^{a,b}**INFN Sezione di Pavia ^a, Università di Pavia ^b, Pavia, Italy**C. Aime^{a,b}, A. Braghieri^a, S. Calzaferri^{a,b}, D. Fiorina^{a,b}, P. Montagna^{a,b}, S.P. Ratti^{a,b}, V. Re^a, M. Ressegotti^{a,b}, C. Riccardi^{a,b}, P. Salvini^a, I. Vai^a, P. Vitulo^{a,b}

INFN Sezione di Perugia ^a, Università di Perugia ^b, Perugia, Italy

M. Biasini^{a,b}, G.M. Bilei^a, D. Ciangottini^{a,b}, L. Fanò^{a,b}, P. Lariccia^{a,b}, G. Mantovani^{a,b}, V. Mariani^{a,b}, M. Menichelli^a, F. Moscatelli^a, A. Piccinelli^{a,b}, A. Rossi^{a,b}, A. Santocchia^{a,b}, D. Spiga^a, T. Tedeschi^{a,b}

INFN Sezione di Pisa ^a, Università di Pisa ^b, Scuola Normale Superiore di Pisa ^c, Pisa Italy, Università di Siena ^d, Siena, Italy

K. Androsov^a, P. Azzurri^a, G. Bagliesi^a, V. Bertacchi^{a,c}, L. Bianchini^a, T. Boccali^a, R. Castaldi^a, M.A. Ciocci^{a,b}, R. Dell'Orso^a, M.R. Di Domenico^{a,b}, S. Donato^a, L. Giannini^{a,c}, A. Giassi^a, M.T. Grippo^a, F. Ligabue^{a,c}, E. Manca^{a,c}, G. Mandorli^{a,c}, A. Messineo^{a,b}, F. Palla^a, G. Ramirez-Sanchez^{a,c}, A. Rizzi^{a,b}, G. Rolandi^{a,c}, S. Roy Chowdhury^{a,c}, A. Scribano^a, N. Shafiei^{a,b}, P. Spagnolo^a, R. Tenchini^a, G. Tonelli^{a,b}, N. Turini^a, A. Venturi^a, P.G. Verdini^a

INFN Sezione di Roma ^a, Sapienza Università di Roma ^b, Rome, Italy

F. Cavallari^a, M. Cipriani^{a,b}, D. Del Re^{a,b}, E. Di Marco^a, M. Diemoz^a, E. Longo^{a,b}, P. Meridiani^a, G. Organtini^{a,b}, F. Pandolfi^a, R. Paramatti^{a,b}, C. Quaranta^{a,b}, S. Rahatlou^{a,b}, C. Rovelli^a, F. Santanastasio^{a,b}, L. Soffi^{a,b}, R. Tramontano^{a,b}

INFN Sezione di Torino ^a, Università di Torino ^b, Torino, Italy, Università del Piemonte Orientale ^c, Novara, Italy

N. Amapane^{a,b}, R. Arcidiacono^{a,c}, S. Argiro^{a,b}, M. Arneodo^{a,c}, N. Bartosik^a, R. Bellan^{a,b}, A. Bellora^{a,b}, J. Berenguer Antequera^{a,b}, C. Biino^a, A. Cappati^{a,b}, N. Cartiglia^a, S. Cometti^a, M. Costa^{a,b}, R. Covarelli^{a,b}, N. Demaria^a, B. Kiani^{a,b}, F. Legger^a, C. Mariotti^a, S. Maselli^a, E. Migliore^{a,b}, V. Monaco^{a,b}, E. Monteil^{a,b}, M. Monteno^a, M.M. Obertino^{a,b}, G. Ortona^a, L. Pacher^{a,b}, N. Pastrone^a, M. Pelliccioni^a, G.L. Pinna Angioni^{a,b}, M. Ruspa^{a,c}, R. Salvatico^{a,b}, F. Siviero^{a,b}, V. Sola^a, A. Solano^{a,b}, D. Soldi^{a,b}, A. Staiano^a, M. Tornago^{a,b}, D. Trocino^{a,b}

INFN Sezione di Trieste ^a, Università di Trieste ^b, Trieste, Italy

S. Belforte^a, V. Candelise^{a,b}, M. Casarsa^a, F. Cossutti^a, A. Da Rold^{a,b}, G. Della Ricca^{a,b}, F. Vazzoler^{a,b}

Kyungpook National University, Daegu, Korea

S. Dogra, C. Huh, B. Kim, D.H. Kim, G.N. Kim, J. Lee, S.W. Lee, C.S. Moon, Y.D. Oh, S.I. Pak, B.C. Radburn-Smith, S. Sekmen, Y.C. Yang

Chonnam National University, Institute for Universe and Elementary Particles, Kwangju, Korea

H. Kim, D.H. Moon

Hanyang University, Seoul, Korea

B. Francois, T.J. Kim, J. Park

Korea University, Seoul, Korea

S. Cho, S. Choi, Y. Go, S. Ha, B. Hong, K. Lee, K.S. Lee, J. Lim, J. Park, S.K. Park, J. Yoo

Kyung Hee University, Department of Physics, Seoul, Republic of Korea

J. Goh, A. Gurtu

Sejong University, Seoul, Korea

H.S. Kim, Y. Kim

Seoul National University, Seoul, Korea

J. Almond, J.H. Bhyun, J. Choi, S. Jeon, J. Kim, J.S. Kim, S. Ko, H. Kwon, H. Lee, K. Lee, S. Lee, K. Nam, B.H. Oh, M. Oh, S.B. Oh, H. Seo, U.K. Yang, I. Yoon

University of Seoul, Seoul, Korea

D. Jeon, J.H. Kim, B. Ko, J.S.H. Lee, I.C. Park, Y. Roh, D. Song, I.J. Watson

Yonsei University, Department of Physics, Seoul, Korea

H.D. Yoo

Sungkyunkwan University, Suwon, Korea

Y. Choi, C. Hwang, Y. Jeong, H. Lee, Y. Lee, I. Yu

College of Engineering and Technology, American University of the Middle East (AUM), Kuwait

Y. Maghrbi

Riga Technical University, Riga, Latvia

V. Veckalns⁴⁸

Vilnius University, Vilnius, Lithuania

A. Juodagalvis, A. Rinkevicius, G. Tamulaitis, A. Vaitkevicius

National Centre for Particle Physics, Universiti Malaya, Kuala Lumpur, Malaysia

W.A.T. Wan Abdullah, M.N. Yusli, Z. Zolkapli

Universidad de Sonora (UNISON), Hermosillo, Mexico

J.F. Benitez, A. Castaneda Hernandez, J.A. Murillo Quijada, L. Valencia Palomo

Centro de Investigacion y de Estudios Avanzados del IPN, Mexico City, Mexico

G. Ayala, H. Castilla-Valdez, E. De La Cruz-Burelo, I. Heredia-De La Cruz⁴⁹, R. Lopez-Fernandez, C.A. Mondragon Herrera, D.A. Perez Navarro, A. Sanchez-Hernandez

Universidad Iberoamericana, Mexico City, Mexico

S. Carrillo Moreno, C. Oropeza Barrera, M. Ramirez-Garcia, F. Vazquez Valencia

Benemerita Universidad Autonoma de Puebla, Puebla, Mexico

J. Eysermans, I. Pedraza, H.A. Salazar Ibarquen, C. Uribe Estrada

Universidad Autónoma de San Luis Potosí, San Luis Potosí, Mexico

A. Morelos Pineda

University of Montenegro, Podgorica, Montenegro

J. Mijuskovic⁴, N. Raicevic

University of Auckland, Auckland, New Zealand

D. Krofcheck

University of Canterbury, Christchurch, New Zealand

S. Bheesette, P.H. Butler

National Centre for Physics, Quaid-I-Azam University, Islamabad, Pakistan

A. Ahmad, M.I. Asghar, A. Awais, M.I.M. Awan, H.R. Hoorani, W.A. Khan, S. Qazi, M.A. Shah, M. Waqas

AGH University of Science and Technology Faculty of Computer Science, Electronics and Telecommunications, Krakow, Poland

V. Avati, L. Grzanka, M. Malawski

National Centre for Nuclear Research, Swierk, Poland

H. Bialkowska, M. Bluj, B. Boimska, T. Frueboes, M. Górski, M. Kazana, M. Szleper, P. Traczyk, P. Zalewski

Institute of Experimental Physics, Faculty of Physics, University of Warsaw, Warsaw, Poland
K. Bunkowski, K. Doroba, A. Kalinowski, M. Konecki, J. Krolikowski, M. Walczak

Laboratório de Instrumentação e Física Experimental de Partículas, Lisboa, Portugal
M. Araujo, P. Bargassa, D. Bastos, A. Boletti, P. Faccioli, M. Gallinaro, J. Hollar, N. Leonardo, T. Niknejad, J. Seixas, K. Shchelina, O. Toldaiev, J. Varela

Joint Institute for Nuclear Research, Dubna, Russia
S. Afanasiev, A. Baginyan, M. Gavrilenko, A. Golunov, I. Golutvin, I. Gorbunov, A. Kamenev, V. Karjavine, I. Kashunin, V. Korenkov, A. Lanev, A. Malakhov, V. Matveev^{50,51}, V. Palichik, V. Perelygin, M. Savina, S. Shmatov, S. Shulha, V. Smirnov, O. Teryaev, N. Voytishin, A. Zarubin

Petersburg Nuclear Physics Institute, Gatchina (St. Petersburg), Russia
G. Gavrillov, V. Golovtsov, Y. Ivanov, V. Kim⁵², E. Kuznetsova⁵³, V. Murzin, V. Oreshkin, I. Smirnov, D. Sosnov, V. Sulimov, L. Uvarov, S. Volkov, A. Vorobyev

Institute for Nuclear Research, Moscow, Russia
Yu. Andreev, A. Dermenev, S. Gninenko, N. Golubev, A. Karneyeu, M. Kirsanov, N. Krasnikov, A. Pashenkov, G. Pivovarov, D. Tlisov[†], A. Toropin

Institute for Theoretical and Experimental Physics named by A.I. Alikhanov of NRC 'Kurchatov Institute', Moscow, Russia
V. Epshteyn, V. Gavrillov, N. Lychkovskaya, A. Nikitenko⁵⁴, V. Popov, G. Safronov, A. Spiridonov, A. Steppenov, M. Toms, E. Vlasov, A. Zhokin

Moscow Institute of Physics and Technology, Moscow, Russia
T. Aushev

National Research Nuclear University 'Moscow Engineering Physics Institute' (MEPhI), Moscow, Russia
R. Chistov⁵⁵, M. Danilov⁵⁶, A. Oskin, P. Parygin, S. Polikarpov⁵⁶

P.N. Lebedev Physical Institute, Moscow, Russia
V. Andreev, M. Azarkin, I. Dremin, M. Kirakosyan, A. Terkulov

Skobeltsyn Institute of Nuclear Physics, Lomonosov Moscow State University, Moscow, Russia
A. Belyaev, E. Boos, V. Bunichev, M. Dubinin⁵⁷, L. Dudko, A. Gribushin, V. Klyukhin, N. Korneeva, I. Lokhtin, S. Obraztsov, M. Perfilov, V. Savrin, P. Volkov

Novosibirsk State University (NSU), Novosibirsk, Russia
V. Blinov⁵⁸, T. Dimova⁵⁸, L. Kardapoltsev⁵⁸, I. Ovtin⁵⁸, Y. Skovpen⁵⁸

Institute for High Energy Physics of National Research Centre 'Kurchatov Institute', Protvino, Russia
I. Azhgirey, I. Bayshev, V. Kachanov, A. Kalinin, D. Konstantinov, V. Petrov, R. Ryutin, A. Sobol, S. Troshin, N. Tyurin, A. Uzunian, A. Volkov

National Research Tomsk Polytechnic University, Tomsk, Russia
A. Babaev, A. Iuzhakov, V. Okhotnikov, L. Sukhikh

Tomsk State University, Tomsk, Russia
V. Borchsh, V. Ivanchenko, E. Tcherniaev

University of Belgrade: Faculty of Physics and VINCA Institute of Nuclear Sciences, Belgrade, Serbia

P. Adzic⁵⁹, M. Dordevic, P. Milenovic, J. Milosevic

Centro de Investigaciones Energéticas Medioambientales y Tecnológicas (CIEMAT), Madrid, Spain

M. Aguilar-Benitez, J. Alcaraz Maestre, A. Álvarez Fernández, I. Bachiller, M. Barrio Luna, Cristina F. Bedoya, C.A. Carrillo Montoya, M. Cepeda, M. Cerrada, N. Colino, B. De La Cruz, A. Delgado Peris, J.P. Fernández Ramos, J. Flix, M.C. Fouz, O. Gonzalez Lopez, S. Goy Lopez, J.M. Hernandez, M.I. Josa, J. León Holgado, D. Moran, Á. Navarro Tobar, A. Pérez-Calero Yzquierdo, J. Puerta Pelayo, I. Redondo, L. Romero, S. Sánchez Navas, M.S. Soares, L. Urda Gómez, C. Willmott

Universidad Autónoma de Madrid, Madrid, Spain

C. Albajar, J.F. de Trocóniz, R. Reyes-Almanza

Universidad de Oviedo, Instituto Universitario de Ciencias y Tecnologías Espaciales de Asturias (ICTEA), Oviedo, Spain

B. Alvarez Gonzalez, J. Cuevas, C. Erice, J. Fernandez Menendez, S. Folgueras, I. Gonzalez Caballero, E. Palencia Cortezon, C. Ramón Álvarez, J. Ripoll Sau, V. Rodríguez Bouza, S. Sanchez Cruz, A. Trapote

Instituto de Física de Cantabria (IFCA), CSIC-Universidad de Cantabria, Santander, Spain

J.A. Brochero Cifuentes, I.J. Cabrillo, A. Calderon, B. Chazin Quero, J. Duarte Campderros, M. Fernandez, P.J. Fernández Manteca, A. García Alonso, G. Gomez, C. Martinez Rivero, P. Martinez Ruiz del Arbol, F. Matorras, J. Piedra Gomez, C. Prieels, F. Ricci-Tam, T. Rodrigo, A. Ruiz-Jimeno, L. Scodellaro, I. Vila, J.M. Vizan Garcia

University of Colombo, Colombo, Sri Lanka

MK Jayananda, B. Kailasapathy⁶⁰, D.U.J. Sonnadara, DDC Wickramarathna

University of Ruhuna, Department of Physics, Matara, Sri Lanka

W.G.D. Dharmaratna, K. Liyanage, N. Perera, N. Wickramage

CERN, European Organization for Nuclear Research, Geneva, Switzerland

T.K. Aarrestad, D. Abbaneo, E. Auffray, G. Auzinger, J. Baechler, P. Baillon, A.H. Ball, D. Barney, J. Bendavid, N. Beni, M. Bianco, A. Bocci, E. Bossini, E. Brondolin, T. Camporesi, M. Capeans Garrido, G. Cerminara, L. Cristella, D. d'Enterria, A. Dabrowski, N. Daci, A. David, A. De Roeck, M. Deile, R. Di Maria, M. Dobson, M. Dünser, N. Dupont, A. Elliott-Peisert, N. Emriskova, F. Fallavollita⁶¹, D. Fasanella, S. Fiorendi, A. Florent, G. Franzoni, J. Fulcher, W. Funk, S. Giani, D. Gigi, K. Gill, F. Glege, L. Gouskos, M. Guilbaud, M. Haranko, J. Hegeman, Y. Iiyama, V. Innocente, T. James, P. Janot, J. Kaspar, J. Kieseler, M. Komm, N. Kratochwil, C. Lange, S. Laurila, P. Lecoq, K. Long, C. Lourenço, L. Malgeri, S. Mallios, M. Mannelli, F. Meijers, S. Mersi, E. Meschi, F. Moortgat, M. Mulders, S. Orfanelli, L. Orsini, F. Pantaleo²², L. Pape, E. Perez, M. Peruzzi, A. Petrilli, G. Petrucciani, A. Pfeiffer, M. Pierini, T. Quast, D. Rabaday, A. Racz, M. Rieger, M. Rovere, H. Sakulin, J. Salfeld-Nebgen, S. Scarfi, C. Schäfer, C. Schwick, M. Selvaggi, A. Sharma, P. Silva, W. Snoeys, P. Sphicas⁶², S. Summers, V.R. Tavolaro, D. Treille, A. Tsirou, G.P. Van Onsem, A. Vartak, M. Verzetti, K.A. Wozniak, W.D. Zeuner

Paul Scherrer Institut, Villigen, Switzerland

L. Caminada⁶³, W. Erdmann, R. Horisberger, Q. Ingram, H.C. Kaestli, D. Kotlinski, U. Langenegger, M. Missiroli, T. Rohe

ETH Zurich - Institute for Particle Physics and Astrophysics (IPA), Zurich, Switzerland

M. Backhaus, P. Berger, A. Calandri, N. Chernyavskaya, A. De Cosa, G. Dissertori, M. Dittmar, M. Donegà, C. Dorfer, T. Gadek, T.A. Gómez Espinosa, C. Grab, D. Hits, W. Luster, M. Lyon, R.A. Manzoni, M.T. Meinhard, F. Micheli, F. Nessi-Tedaldi, J. Niedziela, F. Pauss, V. Perovic, G. Perrin, S. Pigazzini, M.G. Ratti, M. Reichmann, C. Reissel, T. Reitspiess, B. Ristic, D. Ruini, D.A. Sanz Becerra, M. Schönenberger, V. Stampf, J. Steggemann⁶⁴, R. Wallny, D.H. Zhu

Universität Zürich, Zurich, Switzerland

C. AMSLER⁶⁵, C. Botta, D. Brzhechko, M.F. Canelli, R. Del Burgo, J.K. Heikkilä, M. Huwiler, A. Jofrehei, B. Kilminster, S. Leontsinis, A. Macchiolo, P. Meiring, V.M. Mikuni, U. Molinatti, I. Neutelings, G. Rauco, A. Reimers, P. Robmann, K. Schweiger, Y. Takahashi

National Central University, Chung-Li, Taiwan

C. Adloff⁶⁶, C.M. Kuo, W. Lin, A. Roy, T. Sarkar³⁹, S.S. Yu

National Taiwan University (NTU), Taipei, Taiwan

L. Ceard, P. Chang, Y. Chao, K.F. Chen, P.H. Chen, W.-S. Hou, Y.y. Li, R.-S. Lu, E. Paganis, A. Psallidas, A. Steen, E. Yazgan

Chulalongkorn University, Faculty of Science, Department of Physics, Bangkok, Thailand

B. Asavapibhop, C. Asawatangtrakuldee, N. Srimanobhas

Çukurova University, Physics Department, Science and Art Faculty, Adana, Turkey

F. Boran, S. Damarcekin⁶⁷, Z.S. Demiroglu, F. Dolek, C. Dozen⁶⁸, I. Dumanoglu⁶⁹, E. Eskut, G. Gokbulut, Y. Guler, E. Gurpinar Guler⁷⁰, I. Hos⁷¹, C. Isik, E.E. Kangal⁷², O. Kara, A. Kayis Topaksu, U. Kiminsu, G. Onengut, K. Ozdemir⁷³, A. Polatoz, A.E. Simsek, B. Tali⁷⁴, U.G. Tok, S. Turkcapar, I.S. Zorbakir, C. Zorbilmez

Middle East Technical University, Physics Department, Ankara, Turkey

B. Isildak⁷⁵, G. Karapinar⁷⁶, K. Ocalan⁷⁷, M. Yalvac⁷⁸

Bogazici University, Istanbul, Turkey

B. Akgun, I.O. Atakisi, E. Gülmez, M. Kaya⁷⁹, O. Kaya⁸⁰, Ö. Özçelik, S. Tekten⁸¹, E.A. Yetkin⁸²

Istanbul Technical University, Istanbul, Turkey

A. Cakir, K. Cankocak⁶⁹, Y. Komurcu, S. Sen⁸³

Istanbul University, Istanbul, Turkey

F. Aydogmus Sen, S. Cerci⁷⁴, B. Kaynak, S. Ozkorucuklu, D. Sunar Cerci⁷⁴

Institute for Scintillation Materials of National Academy of Science of Ukraine, Kharkov, Ukraine

B. Grynyov

National Scientific Center, Kharkov Institute of Physics and Technology, Kharkov, Ukraine

L. Levchuk

University of Bristol, Bristol, United Kingdom

E. Bhal, S. Bologna, J.J. Brooke, E. Clement, D. Cussans, H. Flacher, J. Goldstein, G.P. Heath, H.F. Heath, L. Kreczko, B. Krikler, S. Paramesvaran, T. Sakuma, S. Seif El Nasr-Storey, V.J. Smith, N. Stylianou⁸⁴, J. Taylor, A. Titterton

Rutherford Appleton Laboratory, Didcot, United Kingdom

K.W. Bell, A. Belyaev⁸⁵, C. Brew, R.M. Brown, D.J.A. Cockerill, K.V. Ellis, K. Harder,

S. Harper, J. Linacre, K. Manolopoulos, D.M. Newbold, E. Olaiya, D. Petyt, T. Reis, T. Schuh, C.H. Shepherd-Themistocleous, A. Thea, I.R. Tomalin, T. Williams

Imperial College, London, United Kingdom

R. Bainbridge, P. Bloch, S. Bonomally, J. Borg, S. Breeze, O. Buchmuller, A. Bundock, V. Cepaitis, G.S. Chahal⁸⁶, D. Colling, P. Dauncey, G. Davies, M. Della Negra, G. Fedi, G. Hall, G. Iles, J. Langford, L. Lyons, A.-M. Magnan, S. Malik, A. Martelli, V. Milosevic, J. Nash⁸⁷, V. Palladino, M. Pesaresi, D.M. Raymond, A. Richards, A. Rose, E. Scott, C. Seez, A. Shtipliyski, M. Stoye, A. Tapper, K. Uchida, T. Virdee²², N. Wardle, S.N. Webb, D. Winterbottom, A.G. Zecchinelli

Brunel University, Uxbridge, United Kingdom

J.E. Cole, P.R. Hobson, A. Khan, P. Kyberd, C.K. Mackay, I.D. Reid, L. Teodorescu, S. Zahid

Baylor University, Waco, USA

S. Abdullin, A. Brinkerhoff, K. Call, B. Caraway, J. Dittmann, K. Hatakeyama, A.R. Kanuganti, C. Madrid, B. McMaster, N. Pastika, S. Sawant, C. Smith, J. Wilson

Catholic University of America, Washington, DC, USA

R. Bartek, A. Dominguez, R. Uniyal, A.M. Vargas Hernandez

The University of Alabama, Tuscaloosa, USA

A. Buccilli, O. Charaf, S.I. Cooper, D. Di Croce, S.V. Gleyzer, C. Henderson, C.U. Perez, P. Rumerio, C. West

Boston University, Boston, USA

A. Akpınar, A. Albert, D. Arcaro, C. Cosby, Z. Demiragli, D. Gastler, J. Rohlf, K. Salyer, D. Sperka, D. Spitzbart, I. Suarez, S. Yuan, D. Zou

Brown University, Providence, USA

G. Benelli, B. Burkle, X. Coubez²³, D. Cutts, Y.t. Duh, M. Hadley, U. Heintz, J.M. Hogan⁸⁸, K.H.M. Kwok, E. Laird, G. Landsberg, K.T. Lau, J. Lee, M. Narain, S. Sagir⁸⁹, R. Syarif, E. Usai, W.Y. Wong, D. Yu, W. Zhang

University of California, Davis, Davis, USA

R. Band, C. Brainerd, R. Breedon, M. Calderon De La Barca Sanchez, M. Chertok, J. Conway, R. Conway, P.T. Cox, R. Erbacher, C. Flores, G. Funk, F. Jensen, W. Ko[†], O. Kukral, R. Lander, M. Mulhearn, D. Pellett, J. Pilot, M. Shi, D. Taylor, K. Tos, M. Tripathi, Y. Yao, F. Zhang

University of California, Los Angeles, USA

M. Bachtis, R. Cousins, A. Dasgupta, D. Hamilton, J. Hauser, M. Ignatenko, M.A. Iqbal, T. Lam, N. Mccoll, W.A. Nash, S. Regnard, D. Saltzberg, C. Schnaible, B. Stone, V. Valuev

University of California, Riverside, Riverside, USA

K. Burt, Y. Chen, R. Clare, J.W. Gary, G. Hanson, G. Karapostoli, O.R. Long, N. Manganeli, M. Olmedo Negrete, W. Si, S. Wimpenny, Y. Zhang

University of California, San Diego, La Jolla, USA

J.G. Branson, P. Chang, S. Cittolin, S. Cooperstein, N. Deelen, J. Duarte, R. Gerosa, D. Gilbert, V. Krutelyov, J. Letts, M. Masciovecchio, S. May, S. Padhi, M. Pieri, V. Sharma, M. Tadel, F. Würthwein, A. Yagil

University of California, Santa Barbara - Department of Physics, Santa Barbara, USA

N. Amin, C. Campagnari, M. Citron, A. Dorsett, V. Dutta, J. Incandela, M. Kilpatrick, B. Marsh, H. Mei, A. Ovcharova, H. Qu, M. Quinnan, J. Richman, U. Sarica, D. Stuart, S. Wang

California Institute of Technology, Pasadena, USA

A. Bornheim, O. Cerri, I. Dutta, J.M. Lawhorn, N. Lu, J. Mao, H.B. Newman, J. Ngadiuba, T.Q. Nguyen, M. Spiropulu, J.R. Vlimant, C. Wang, S. Xie, Z. Zhang, R.Y. Zhu

Carnegie Mellon University, Pittsburgh, USA

J. Alison, M.B. Andrews, T. Ferguson, T. Mudholkar, M. Paulini, I. Vorobiev

University of Colorado Boulder, Boulder, USA

J.P. Cumalat, W.T. Ford, E. MacDonald, R. Patel, A. Perloff, K. Stenson, K.A. Ulmer, S.R. Wagner

Cornell University, Ithaca, USA

J. Alexander, Y. Cheng, J. Chu, D.J. Cranshaw, A. Datta, A. Frankenthal, K. Mcdermott, J. Monroy, J.R. Patterson, D. Quach, A. Ryd, W. Sun, S.M. Tan, Z. Tao, J. Thom, P. Wittich, M. Zientek

Fermi National Accelerator Laboratory, Batavia, USA

M. Albrow, M. Alyari, G. Apollinari, A. Apresyan, A. Apyan, S. Banerjee, L.A.T. Bauerdick, A. Beretvas, D. Berry, J. Berryhill, P.C. Bhat, K. Burkett, J.N. Butler, A. Canepa, G.B. Cerati, H.W.K. Cheung, F. Chlebana, M. Cremonesi, K.F. Di Petrillo, V.D. Elvira, J. Freeman, Z. Gecse, L. Gray, D. Green, S. Grünendahl, O. Gutsche, R.M. Harris, S. Hasegawa, R. Heller, T.C. Herwig, J. Hirschauer, B. Jayatilaka, S. Jindariani, M. Johnson, U. Joshi, P. Klabbers, T. Klijnsma, B. Klima, M.J. Kortelainen, S. Lammel, D. Lincoln, R. Lipton, M. Liu, T. Liu, J. Lykken, K. Maeshima, D. Mason, P. McBride, P. Merkel, S. Mrenna, S. Nahn, V. O'Dell, V. Papadimitriou, K. Pedro, C. Pena⁵⁷, O. Prokofyev, F. Ravera, A. Reinsvold Hall, L. Ristori, B. Schneider, E. Sexton-Kennedy, N. Smith, A. Soha, W.J. Spalding, L. Spiegel, S. Stoynev, J. Strait, L. Taylor, S. Tkaczyk, N.V. Tran, L. Uplegger, E.W. Vaandering, H.A. Weber

University of Florida, Gainesville, USA

D. Acosta, P. Avery, D. Bourilkov, L. Cadamuro, V. Cherepanov, F. Errico, R.D. Field, D. Guerrero, B.M. Joshi, M. Kim, J. Konigsberg, A. Korytov, K.H. Lo, K. Matchev, N. Menendez, G. Mitselmakher, D. Rosenzweig, K. Shi, J. Sturdy, J. Wang, X. Zuo

Florida State University, Tallahassee, USA

T. Adams, A. Askew, D. Diaz, R. Habibullah, S. Hagopian, V. Hagopian, K.F. Johnson, R. Khurana, T. Kolberg, G. Martinez, H. Prosper, C. Schiber, R. Yohay, J. Zhang

Florida Institute of Technology, Melbourne, USA

M.M. Baarmand, S. Butalla, T. Elkafrawy¹⁶, M. Hohlmann, D. Noonan, M. Rahmani, M. Saunders, F. Yumiceva

University of Illinois at Chicago (UIC), Chicago, USA

M.R. Adams, L. Apanasevich, H. Becerril Gonzalez, R. Cavanaugh, X. Chen, S. Dittmer, O. Evdokimov, C.E. Gerber, D.A. Hangal, D.J. Hofman, C. Mills, G. Oh, T. Roy, M.B. Tonjes, N. Varelas, J. Viinikainen, X. Wang, Z. Wu, Z. Ye

The University of Iowa, Iowa City, USA

M. Alhousseini, K. Dilsiz⁹⁰, S. Durgut, R.P. Gandrajula, M. Haytmyradov, V. Khristenko, O.K. Köseyan, J.-P. Merlo, A. Mestvirishvili⁹¹, A. Moeller, J. Nachtman, H. Ogul⁹², Y. Onel, E. Ozok⁹³, A. Penzo, C. Snyder, E. Tiras⁹⁴, J. Wetzel

Johns Hopkins University, Baltimore, USA

O. Amram, B. Blumenfeld, L. Corcodilos, M. Eminizer, A.V. Gritsan, S. Kyriacou, P. Maksimovic, C. Mantilla, J. Roskes, M. Swartz, T.Á. Vámi

The University of Kansas, Lawrence, USA

C. Baldenegro Barrera, P. Baringer, A. Bean, A. Bylinkin, T. Isidori, S. Khalil, J. King, G. Krintiras, A. Kropivnitskaya, C. Lindsey, N. Minafra, M. Murray, C. Rogan, C. Royon, S. Sanders, E. Schmitz, J.D. Tapia Takaki, Q. Wang, J. Williams, G. Wilson

Kansas State University, Manhattan, USA

S. Duric, A. Ivanov, K. Kaadze, D. Kim, Y. Maravin, T. Mitchell, A. Modak, A. Mohammadi

Lawrence Livermore National Laboratory, Livermore, USA

F. Rebassoo, D. Wright

University of Maryland, College Park, USA

E. Adams, A. Baden, O. Baron, A. Belloni, S.C. Eno, Y. Feng, N.J. Hadley, S. Jabeen, G.Y. Jeng, R.G. Kellogg, T. Koeth, A.C. Mignerey, S. Nabili, M. Seidel, A. Skuja, S.C. Tonwar, L. Wang, K. Wong

Massachusetts Institute of Technology, Cambridge, USA

D. Abercrombie, B. Allen, R. Bi, S. Brandt, W. Busza, I.A. Cali, Y. Chen, M. D'Alfonso, G. Gomez Ceballos, M. Goncharov, P. Harris, D. Hsu, M. Hu, M. Klute, D. Kovalskyi, J. Krupa, Y.-J. Lee, P.D. Luckey, B. Maier, A.C. Marini, C. Mironov, S. Narayanan, X. Niu, C. Paus, D. Rankin, C. Roland, G. Roland, Z. Shi, G.S.F. Stephans, K. Sumorok, K. Tatar, D. Velicanu, J. Wang, T.W. Wang, Z. Wang, B. Wyslouch

University of Minnesota, Minneapolis, USA

R.M. Chatterjee, A. Evans, P. Hansen, J. Hiltbrand, Sh. Jain, M. Krohn, Y. Kubota, Z. Lesko, J. Mans, M. Revering, R. Rusack, R. Saradhy, N. Schroeder, N. Strobbe, M.A. Wadud

University of Mississippi, Oxford, USA

J.G. Acosta, S. Oliveros

University of Nebraska-Lincoln, Lincoln, USA

K. Bloom, S. Chauhan, D.R. Claes, C. Fangmeier, L. Finco, F. Golf, J.R. González Fernández, C. Joo, I. Kravchenko, J.E. Siado, G.R. Snow[†], W. Tabb, F. Yan

State University of New York at Buffalo, Buffalo, USA

G. Agarwal, H. Bandyopadhyay, L. Hay, I. Iashvili, A. Kharchilava, C. McLean, D. Nguyen, J. Pekkanen, S. Rappoccio

Northeastern University, Boston, USA

G. Alverson, E. Barberis, C. Freer, Y. Haddad, A. Hortiangtham, J. Li, G. Madigan, B. Marzocchi, D.M. Morse, V. Nguyen, T. Orimoto, A. Parker, L. Skinnari, A. Tishelman-Charny, T. Wamorkar, B. Wang, A. Wisecarver, D. Wood

Northwestern University, Evanston, USA

S. Bhattacharya, J. Bueghly, Z. Chen, A. Gilbert, T. Gunter, K.A. Hahn, N. Odell, M.H. Schmitt, K. Sung, M. Velasco

University of Notre Dame, Notre Dame, USA

R. Bucci, N. Dev, R. Goldouzian, M. Hildreth, K. Hurtado Anampa, C. Jessop, K. Lannon, N. Loukas, N. Marinelli, I. Mcalister, F. Meng, K. Mohrman, Y. Musienko⁵⁰, R. Ruchti, P. Siddireddy, M. Wayne, A. Wightman, M. Wolf, L. Zygala

The Ohio State University, Columbus, USA

J. Alimena, B. Bylsma, B. Cardwell, L.S. Durkin, B. Francis, C. Hill, A. Lefeld, B.L. Winer, B.R. Yates

Princeton University, Princeton, USA

B. Bonham, P. Das, G. Dezoort, P. Elmer, B. Greenberg, N. Haubrich, S. Higginbotham, A. Kalogeropoulos, G. Kopp, S. Kwan, D. Lange, M.T. Lucchini, J. Luo, D. Marlow, K. Mei, I. Ojalvo, J. Olsen, C. Palmer, P. Piroué, D. Stickland, C. Tully

University of Puerto Rico, Mayaguez, USA

S. Malik, S. Norberg

Purdue University, West Lafayette, USA

V.E. Barnes, R. Chawla, S. Das, L. Gutay, M. Jones, A.W. Jung, G. Negro, N. Neumeister, C.C. Peng, S. Piperov, A. Purohit, J.F. Schulte, M. Stojanovic¹⁸, N. Trevisani, F. Wang, A. Wildridge, R. Xiao, W. Xie

Purdue University Northwest, Hammond, USA

J. Dolen, N. Parashar

Rice University, Houston, USA

A. Baty, S. Dildick, K.M. Ecklund, S. Freed, F.J.M. Geurts, A. Kumar, W. Li, B.P. Padley, R. Redjimi, J. Roberts[†], J. Rorie, W. Shi, A.G. Stahl Leiton

University of Rochester, Rochester, USA

A. Bodek, P. de Barbaro, R. Demina, J.L. Dulemba, C. Fallon, T. Ferbel, M. Galanti, A. Garcia-Bellido, O. Hindrichs, A. Khukhunaishvili, E. Ranken, R. Taus

Rutgers, The State University of New Jersey, Piscataway, USA

B. Chiarito, J.P. Chou, A. Gandrakota, Y. Gershtein, E. Halkiadakis, A. Hart, M. Heindl, E. Hughes, S. Kaplan, O. Karacheban²⁶, I. Laflotte, A. Lath, R. Montalvo, K. Nash, M. Osherson, S. Salur, S. Schnetzer, S. Somalwar, R. Stone, S.A. Thayil, S. Thomas, H. Wang

University of Tennessee, Knoxville, USA

H. Acharya, A.G. Delannoy, S. Spanier

Texas A&M University, College Station, USA

O. Bouhali⁹⁵, M. Dalchenko, A. Delgado, R. Eusebi, J. Gilmore, T. Huang, T. Kamon⁹⁶, H. Kim, S. Luo, S. Malhotra, R. Mueller, D. Overton, L. Perniè, D. Rathjens, A. Safonov

Texas Tech University, Lubbock, USA

N. Akchurin, J. Damgov, V. Hegde, S. Kunori, K. Lamichhane, S.W. Lee, T. Mengke, S. Muthumuni, T. Peltola, S. Undleeb, I. Volobouev, Z. Wang, A. Whitbeck

Vanderbilt University, Nashville, USA

E. Appelt, S. Greene, A. Gurrola, R. Janjam, W. Johns, C. Maguire, A. Melo, H. Ni, K. Padeken, F. Romeo, P. Sheldon, S. Tuo, J. Velkovska

University of Virginia, Charlottesville, USA

M.W. Arenton, B. Cox, G. Cummings, J. Hakala, R. Hirosky, M. Joyce, A. Ledovskoy, A. Li, C. Neu, B. Tannenwald, E. Wolfe

Wayne State University, Detroit, USA

P.E. Karchin, N. Poudyal, P. Thapa

University of Wisconsin - Madison, Madison, WI, USA

K. Black, T. Bose, J. Buchanan, C. Caillol, S. Dasu, I. De Bruyn, P. Everaerts, C. Galloni, H. He, M. Herndon, A. Hervé, U. Hussain, A. Lanaro, A. Loeliger, R. Loveless, J. Madhusudanan Sreekala, A. Mallampalli, D. Pinna, A. Savin, V. Shang, V. Sharma, W.H. Smith, D. Teague, S. Trembath-reichert, W. Vetens

†: Deceased

- 1: Also at Vienna University of Technology, Vienna, Austria
- 2: Also at Institute of Basic and Applied Sciences, Faculty of Engineering, Arab Academy for Science, Technology and Maritime Transport, Alexandria, Egypt, Alexandria, Egypt
- 3: Also at Université Libre de Bruxelles, Bruxelles, Belgium
- 4: Also at IRFU, CEA, Université Paris-Saclay, Gif-sur-Yvette, France
- 5: Also at Universidade Estadual de Campinas, Campinas, Brazil
- 6: Also at Federal University of Rio Grande do Sul, Porto Alegre, Brazil
- 7: Also at UFMS, Nova Andradina, Brazil
- 8: Also at Universidade Federal de Pelotas, Pelotas, Brazil
- 9: Also at Nanjing Normal University Department of Physics, Nanjing, China
- 10: Now at The University of Iowa, Iowa City, USA
- 11: Also at University of Chinese Academy of Sciences, Beijing, China
- 12: Also at Institute for Theoretical and Experimental Physics named by A.I. Alikhanov of NRC 'Kurchatov Institute', Moscow, Russia
- 13: Also at Joint Institute for Nuclear Research, Dubna, Russia
- 14: Also at Helwan University, Cairo, Egypt
- 15: Now at Zewail City of Science and Technology, Zewail, Egypt
- 16: Also at Ain Shams University, Cairo, Egypt
- 17: Now at British University in Egypt, Cairo, Egypt
- 18: Also at Purdue University, West Lafayette, USA
- 19: Also at Université de Haute Alsace, Mulhouse, France
- 20: Also at Tbilisi State University, Tbilisi, Georgia
- 21: Also at Erzincan Binali Yildirim University, Erzincan, Turkey
- 22: Also at CERN, European Organization for Nuclear Research, Geneva, Switzerland
- 23: Also at RWTH Aachen University, III. Physikalisches Institut A, Aachen, Germany
- 24: Also at University of Hamburg, Hamburg, Germany
- 25: Also at Department of Physics, Isfahan University of Technology, Isfahan, Iran, Isfahan, Iran
- 26: Also at Brandenburg University of Technology, Cottbus, Germany
- 27: Also at Skobeltsyn Institute of Nuclear Physics, Lomonosov Moscow State University, Moscow, Russia
- 28: Also at Institute of Physics, University of Debrecen, Debrecen, Hungary, Debrecen, Hungary
- 29: Also at Physics Department, Faculty of Science, Assiut University, Assiut, Egypt
- 30: Also at Eszterhazy Karoly University, Karoly Robert Campus, Gyongyos, Hungary
- 31: Also at Institute of Nuclear Research ATOMKI, Debrecen, Hungary
- 32: Also at MTA-ELTE Lendület CMS Particle and Nuclear Physics Group, Eötvös Loránd University, Budapest, Hungary, Budapest, Hungary
- 33: Also at Wigner Research Centre for Physics, Budapest, Hungary
- 34: Also at IIT Bhubaneswar, Bhubaneswar, India, Bhubaneswar, India
- 35: Also at Institute of Physics, Bhubaneswar, India
- 36: Also at G.H.G. Khalsa College, Punjab, India
- 37: Also at Shoolini University, Solan, India
- 38: Also at University of Hyderabad, Hyderabad, India
- 39: Also at University of Visva-Bharati, Santiniketan, India
- 40: Also at Indian Institute of Technology (IIT), Mumbai, India
- 41: Also at Deutsches Elektronen-Synchrotron, Hamburg, Germany
- 42: Also at Sharif University of Technology, Tehran, Iran

-
- 43: Also at Department of Physics, University of Science and Technology of Mazandaran, Behshahr, Iran
- 44: Now at INFN Sezione di Bari ^a, Università di Bari ^b, Politecnico di Bari ^c, Bari, Italy
- 45: Also at Italian National Agency for New Technologies, Energy and Sustainable Economic Development, Bologna, Italy
- 46: Also at Centro Siciliano di Fisica Nucleare e di Struttura Della Materia, Catania, Italy
- 47: Also at Università di Napoli 'Federico II', NAPOLI, Italy
- 48: Also at Riga Technical University, Riga, Latvia, Riga, Latvia
- 49: Also at Consejo Nacional de Ciencia y Tecnología, Mexico City, Mexico
- 50: Also at Institute for Nuclear Research, Moscow, Russia
- 51: Now at National Research Nuclear University 'Moscow Engineering Physics Institute' (MEPhI), Moscow, Russia
- 52: Also at St. Petersburg State Polytechnical University, St. Petersburg, Russia
- 53: Also at University of Florida, Gainesville, USA
- 54: Also at Imperial College, London, United Kingdom
- 55: Also at Moscow Institute of Physics and Technology, Moscow, Russia, Moscow, Russia
- 56: Also at P.N. Lebedev Physical Institute, Moscow, Russia
- 57: Also at California Institute of Technology, Pasadena, USA
- 58: Also at Budker Institute of Nuclear Physics, Novosibirsk, Russia
- 59: Also at Faculty of Physics, University of Belgrade, Belgrade, Serbia
- 60: Also at Trincomalee Campus, Eastern University, Sri Lanka, Nilaveli, Sri Lanka
- 61: Also at INFN Sezione di Pavia ^a, Università di Pavia ^b, Pavia, Italy, Pavia, Italy
- 62: Also at National and Kapodistrian University of Athens, Athens, Greece
- 63: Also at Universität Zürich, Zurich, Switzerland
- 64: Also at Ecole Polytechnique Fédérale Lausanne, Lausanne, Switzerland
- 65: Also at Stefan Meyer Institute for Subatomic Physics, Vienna, Austria, Vienna, Austria
- 66: Also at Laboratoire d'Annecy-le-Vieux de Physique des Particules, IN2P3-CNRS, Annecy-le-Vieux, France
- 67: Also at Şırnak University, Sirnak, Turkey
- 68: Also at Department of Physics, Tsinghua University, Beijing, China, Beijing, China
- 69: Also at Near East University, Research Center of Experimental Health Science, Nicosia, Turkey
- 70: Also at Beykent University, Istanbul, Turkey, Istanbul, Turkey
- 71: Also at Istanbul Aydin University, Application and Research Center for Advanced Studies (App. & Res. Cent. for Advanced Studies), Istanbul, Turkey
- 72: Also at Mersin University, Mersin, Turkey
- 73: Also at Piri Reis University, Istanbul, Turkey
- 74: Also at Adiyaman University, Adiyaman, Turkey
- 75: Also at Ozyegin University, Istanbul, Turkey
- 76: Also at Izmir Institute of Technology, Izmir, Turkey
- 77: Also at Necmettin Erbakan University, Konya, Turkey
- 78: Also at Bozok Universitetesi Rektörlüğü, Yozgat, Turkey, Yozgat, Turkey
- 79: Also at Marmara University, Istanbul, Turkey
- 80: Also at Milli Savunma University, Istanbul, Turkey
- 81: Also at Kafkas University, Kars, Turkey
- 82: Also at Istanbul Bilgi University, Istanbul, Turkey
- 83: Also at Hacettepe University, Ankara, Turkey
- 84: Also at Vrije Universiteit Brussel, Brussel, Belgium
- 85: Also at School of Physics and Astronomy, University of Southampton, Southampton,

United Kingdom

86: Also at IPPP Durham University, Durham, United Kingdom

87: Also at Monash University, Faculty of Science, Clayton, Australia

88: Also at Bethel University, St. Paul, Minneapolis, USA, St. Paul, USA

89: Also at Karamanoğlu Mehmetbey University, Karaman, Turkey

90: Also at Bingol University, Bingol, Turkey

91: Also at Georgian Technical University, Tbilisi, Georgia

92: Also at Sinop University, Sinop, Turkey

93: Also at Mimar Sinan University, Istanbul, Istanbul, Turkey

94: Also at Erciyes University, KAYSERI, Turkey

95: Also at Texas A&M University at Qatar, Doha, Qatar

96: Also at Kyungpook National University, Daegu, Korea, Daegu, Korea